Towards the Design of Small, Inexpensive, Cable-Driven Dynamic Quadrupedal Robots

by

Jacob Ridgway

A thesis submitted in conformity with the requirements
for the degree of Master of Applied Science

Institute for Aerospace Studies
University of Toronto

Towards the Design of Small, Inexpensive, Cable-Driven Dynamic Quadrupedal Robots

Jacob Ridgway
Master of Applied Science

Institute for Aerospace Studies
University of Toronto
2023

Abstract

There has been a trend towards ever smaller and more capable quadruped robots. Continuing this trend, however, will require the use of smaller, higher-speed electric motors, which in turn will require the use of higher reduction ratio transmissions. Existing transmission designs are unable to achieve these ratios due to excessive friction, inertia, and size, but a cable-driven capstan could solve all of these problems. This project aims to demonstrate the suitability of this design for small quadruped robots by designing, simulating, and testing a physical prototype. Appropriate control methods will be developed and adapted. The resulting quadruped will be significantly lighter and cheaper than the state of the art.

Acknowledgements

I am grateful to my supervisor and committee for their advice and guidance.

I would like thank my family for their support, my friend Zhiye for her encouragement to actually get to writing, Kim for her help with organization, and to Jennifer for her endless patience and love.

Contents

List of Figures

Chapter 1

Introduction

1.1 Thesis Outline

The thesis is divided into six chapters.

The first provides an introduction to quadruped robotics, an overview of the field, and identifies the research gap of a low-cost agile quadruped. It also proposes a design based around a low-cost brushed DC motor, supported by the development of a high reduction ratio backdrivable capstan drive transmission and a nonlinear gravity compensation system.

The second discusses the importance of mechanical impedance matching in more depth, and discusses the advantages of the capstan transmission compared to transmission types that are currently popular in quadruped robotics.

The third discusses the importance of gravity compensation, and challenges with conventional approaches to gravity compensating particularly for mobile robots. It then proposes a novel configuration of springs and links which produce a near-constant force, effectively canceling the effect of gravity over a wide displacement.

The fourth discusses 3D printing as a manufacturing technology and compares it to conventional approaches to manufacturing. It then discusses various techniques to best take advantage of 3D printing's unique capabilities to create stiff and lightweight structures, and shows how they can be applied to a 3D printed quadruped leg prototype.

The fifth discusses the various numerical simulations, analyses, and prototypes that were made in support of the previous topics.

The sixth provides a conclusion and suggestions for future work.

1.2 Introduction

Wheeled robots have excellent endurance and payload, and are easy to build and control, but cannot travel over rough terrain or obstacles like stairs, rendering much of the natural and built environment inaccessible [34] [1] [6]. Quadrotors can fly over obstacles, but have low payload and endurance and struggle in small spaces [1]. Although more complex and difficult to control, legged robots combine decent payload and endurance with the ability to climb stairs and operate in rough terrain and tight spaces, giving full access to the natural and man-made environment.

Animals move using muscles, which have high force and natural compliance, making them a nearly ideal actuator for a legged creature. Despite muscles having a power density far lower than an electric motor, mammals are known for their speed, agility, and endurance [45]. Electric motors operate with low force and high speed—the opposite of muscles—making it difficult to use them as actuators for legged robots directly. A transmission suitable for electric motors must increase torque but keep compliance, a problem for which many different solutions have been proposed.

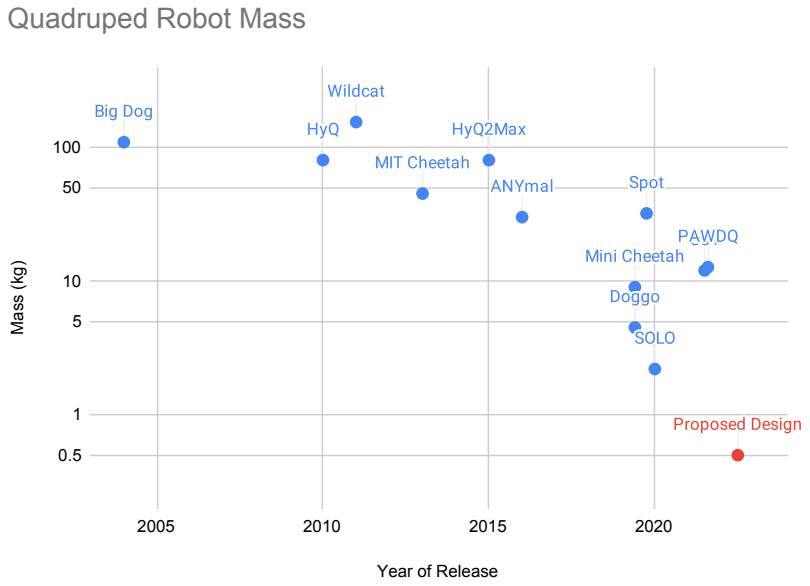

Figure 1.1: The mass of dynamic backdrivable quadruped robots has decreased over time. The Solo-8 robot from the Open Dynamic Robotics Initiative is the current record-holder at 2.2 kg [13]

There is a trend towards smaller and lighter quadrupeds (see Figure 1.1), as they tend to be cheaper, safer, and more agile. Hydraulic actuators, as used in HyQ [35][38][37], HyQ2Max [36], BigDog [34], and Wildcat[1] provide good torque density but are unsuitable for small robots due to being heavy and bulky [1]. Series elastic actuators (SEA), as seen in StarlETH [16] and ANYmal

[1] https://www.bostondynamics.com/legacy

[17] allow high-ratio gearboxes to have compliance, but sacrifice control bandwidth (the spring acts as a low-pass filter) and impedance adjustability. Recent dynamic quadrupeds use quasi-direct drive (QDD), which pairs a high-torque electric motor with a low-reduction-ratio transmission — a planetary gearbox for MIT Cheetah 1-3 [3], Mini Cheetah [21], and PAWDQ [24], and a toothed belt for Stanford Doggo [22] and Solo-8/-12 [13]. To continue making ever smaller robots, smaller, higher-speed motors requiring larger reduction ratios must be used, but the friction, inertia, and bulk of producing the required ratio using gears or even belts becomes prohibitive. One potential solution to these problems is a cable capstan drive.

1.3 Literature Review

High ratio gear drives were initially used to actuate industrial robot arms, where extreme stiffness and strength were required to position parts accurately and support the massive weight of the arms themselves [17]. However, these joints cannot be backdriven, preventing the natural flow of energy into and out of the leg during walking, resulting in stilted gaits [17]. Force sensors are also required because (easily measurable) motor torques no longer represent the true joint torque [17]. Despite its limitations, this approach is popular with many small quadruped designs in the research community and the hobbyist community due to the ubiquity of cheap R/C aircraft servomotors [42] [32].

A logical next step was to use the hydraulic cylinder. Like a muscle, it has very high force density and is capable of being backdriven, and with high speed valves can be controlled with precision. BigDog (2008) [34] had gasoline-powered hydraulics, and HyQ used electricity to power its pump [35][38]. These robots were both about 100 kg. Hydraulics cannot be used on smaller robots due to their weight and complexity [1].

StarlETH took a biologically-inspired approach, combining a high-ratio gearmotor with an spring in series with it. Like a tendon, the spring can stretch to store energy and provide compliance, and the spring's extension provides an easy force measurement. The result was a highly-successful design [1] [16] [17]. The limitations are that compliance introduced between the motor and foot acts as a low-pass filter, resulting in much lower actuator control bandwidth than more rigidly connected designs, and the amount of compliance cannot be altered without mechanical changes [13].

The other extreme is to use a direct drive electrical actuator, in which the motor is rigidly

attached to the leg without any kind of speed reduction. This was the approach taken on the Minitaur and Jerboa. The transparency is maximized, and the lack of any transmission reduces weight and inertia. However, in order to achieve the levels of torque required to support its own weight, the motor must be quite large and heavy due to the lack of any speed reduction, and also during operation only a small fraction of the motor's potential output power will be utilized due to the low speed. In practice, such designs must devote a huge fraction of their mass to motors (40% in the case of Minitaur and Jerboa) and may end up underpowered and overweight [22] [23].

A more promising approach is that of quasi-direct-drive (QDD). The idea is to use a relatively moderate reduction ratio, typically less than 10:1, to substantially increase the torque while not increasing the reflected inertia, friction, and backlash too much, and so get the best of both worlds. One of the first implementations of this concept was the MIT Cheetah series of quadrupeds, which integrate a single stage planetary gearbox with the motor unit for a reduction ratio of 5.8 for Cheetah 2, and 7.67 for Cheetah 3 [39][3]. Although gears do introduce some friction and backlash, this was found to have minimal impact on robot capabilities. The bigger problem was with reflected inertia. Due to the high gear ratio, the reflected inertia of the motor and gears was substantial, and combined with a relatively stiff leg, the peak loads experienced by the transmission during impact of the leg with the ground were much higher than the peak force exerted by the motor itself. Since all the force in a gear gets concentrated on a single tooth, relatively large and heavy gears were required to supply the needed strength, significantly increasing the total mass and inertia of the actuator, and partly cancelling the beneficial effects of the QDD design. In addition to the MIT Cheetah 1-3 and Mini Cheetah [21], a number of other quadrupeds have taken a very similar approach, such as the PAWDQ [24], and the recent robots from Unitree[2]

An improvement on this concept is the belt-driven QDD quadruped. In this approach, a toothed timing belt replaces the planetary gearbox of the MIT Cheetah-style actuator. Because more teeth are engaged simultaneously, a much lighter plastic main wheel can be used, combined with a reinforced rubber belt and a small metal pinion, and can achieve the same torque transfer with lower mass and inertia. The Stanford Doggo uses a single-stage 3:1 belt reduction to achieve superior jump performance [22], and the SOLO robot uses a two stage belt reduction with a 9:1 overall ratio and also achieves excellent jump performance [13]. This is the current state of the art in dynamic quadruped robot actuator design.

To date, SOLO is the lightest quadruped, at 2.5 kg for the full 12-DoF model, to qualify as a fully-dynamic backdrivable system; all lighter robots have used some variation on the highly-

[2] https://www.unitree.com/

geared servomotor concept, some with series elastic elements [e.g. 42]. The challenge with going lighter is that smaller motors tend to have higher natural speeds, requiring greater reduction ratios to increase the torque to a usable level. This is difficult because the reduction methods that were successful at modest reduction ratios start becoming impractical at higher reduction ratios and it is for this reason that Kau et al. [22] restricted their definition of quasi-direct drive to a single-stage reduction of less than 10:1.

Although the increased reduction ratio does not directly increase reflected inertia (as it enables lower-inertia motors to be used) [22], it does increase the peak forces the transmission must be able to take [21]. As toothed belts can only carry a force depending on the number of teeth engaged, the drive pinion cannot shrink any further, so any increases in reduction ratio must come from either making the driven wheel larger or from increasing the number of stages. Neither of these is ideal, since more stages will result in increased friction and play, and larger wheels will have increased inertia and increased packaging difficulty. Furthermore, when scaling down to extremely small scales, very small belts are not available. Similarly, gear teeth cannot be reduced in size without decreasing the strength, and the minimum number of teeth is determined by geometry and the need for smooth running. And even more so than with belts, additional stages of gears will drastically increase the inertia, friction, and backlash of the transmission. These also require intricate geometries that cannot be 3D printed at a small scale.

There does in fact exist a transmission that combines high strength, low weight/inertia, easy fabricability, and extreme reduction ratios in a single stage and moderate size: the capstan cable drive. Cable-drives are ancient, used by the Romans in cranes to haul building materials to the top of a building under construction, by mariners to control sails and deflect the rudder, and in steam shovels before modern hydraulics became common. Their extreme strength-to-weight ratio has made them increasingly popular in robotics too, in robot arms [25][41], medical robots [9], and, due to their unusually high efficiency and transparency, in haptic feedback devices for tele-operation [11] [12]. This last property makes cable drives particularly well suited to backdrivable quadrupeds, as it allows a much higher reduction ratio to be tolerated than otherwise possible. Furthermore, since the pinion side of the capstan drive (the capstan) is a simple cylinder, its radius can be as small as the cable can wrap around. Combined with the use of extremely strong and thin ultra-high-molecular-weight polyethylene (UHMWPE) braids which can safely bend almost any radius, a capstan radius of 1-2 mm is possible, an order of magnitude better than possible with gears or belts, and thanks to the exponential magic of the Eytelwein equation $T_{load} = T_{hold}e^{\mu\phi}$[27], a few wraps of the cable can sustain any load imaginable, so slipping will never be a problem no

matter how small the radius or how poor the friction coefficient.

Cable-drives for quadruped robots have been proposed before. [26][19]. However RoboCat uses series elastic elements, with the attendant loss of control bandwidth, and Stanley [30][31] only has a moderate reduction ratio. Stanley is also a large robot, closer in size to Spot Mini than SOLO or other small quadrupeds. The Capler leg demonstrator project is probably the closest in conception to what is proposed here, in that it takes advantage of UHMWPE capstan transmission. However, it is a much larger leg, fails to take full advantage of the design's potential to create higher reduction ratios and also does not attempt to pursue an ultra-small design [19].

My project will be to combine the best aspects of analysis and design from all the above papers, and build the smallest and cheapest dynamic backdrivable quadruped capable of climbing stairs, using a leg design similar to Stanford Doggo and a transmission similar to Stanley and Capler.

1.4 Project Overview and Methodology

The goal of the project is to explore the concept the use of a high ratio capstan drive and elastic gravity compensation towards furthering the ultimate goal of making a low cost agile 3D printed quadruped robot.

The robot is designed around the Pololu 1592[3], an extremely inexpensive 16 g brushed DC motor with a short lifetime and surprisingly good torque (see Figure A.1). To keep the total motor mass (192 g) more than 40% of the total (to achieve good performance [22][23]), the total mass must remain under 480 g, necessitating use of lightweight batteries, sensors, electronics, and structure. Each leg consists of a 2-DoF Symmetric Parallel SCARA unit [20][22] powered by an integrated single-stage 31:1 capstan reducer mounted directly on the motor shaft, matching the rotational inertia with robot weight for maximum power transfer. Shaft angle is measured with a magnetic encoder or with a 3D printed codewheel optical encoder. This unit can then rotate about a horizontal axis to provide hip adduction/abduction, powered by a third capstan reducer. In contrast with SEA used on StarlETH [16] and ANYmal [17], a parallel elastic element is used to provide stability in the event of power loss and passive gravity compensation during operation, increasing efficiency and performance. The back of the chassis is rounded so that the dog passively returns to feet-down orientation, and the belly is left open for a future manipulator arm.

The sensor package will include an IMU, encoders and current sensors on all motors, foot con-

[3] https://www.pololu.com/product/1592

tact sensors similar to Grimminger et al. [13], and possibly an ultrasonic sensor, laser rangefinder, or camera for navigation or environmental monitoring. Initially an off-the-shelf motor driver will be used, but will be upgraded to a custom MOSFET design to allow for higher current. Computation for high level planning will be provided by the Raspberry Pi Zero 2 W, which integrates 512 MB RAM and a 4-core 1 GHz ARM processor with radio and other peripherals in a small 11 g package, and an ESP32 microcontroller will be used for low-level control and sensor interfacing.

Analysis and simulations will be performed in MATLAB to evaluate the motion dynamics and impedance matching, the workspace geometry and gravity compensation, and control.

Chapter 2

Impedance Matching

2.1 Importance of Impedance Matching in Mechanical Systems

When designing an electromechanical system, the inertia characteristics of the load and the motor can be very different, and in order to effectively drive the load while operating the motor at its optimal speed, it is often necessary to introduce a transmission system, such as a gearbox. This introduces a fixed ratio between the motions of the motor shaft and the load. When selecting the optimal ratio for the transmission of an agile robotic actuator such as for a quadruped robot leg, there are three primary and somewhat contradictory considerations: payload capacity, transparency, and power transfer.

Payload capacity is the most straightforward: the leg must be able to exert enough force to support its own weight, the rest of the robot, any payload, and any dynamic forces. If the motor cannot output enough torque directly, the torque must be increased using some sort of a speed reducing transmission such as a gearbox. Traditionally this has been the main limiting factor in robotics, and many robot joints use high-ratio gearboxes to maximize the torque and stiffness available. This approach was also taken for early humanoid robots, but as a result they had slow and static motions and little ability to undertake dynamic motions like running or jumping as a result of poor transparency and power transfer.

Transparency, also known as backdrivability, is the ability of forces on the end effector to go back through the transmission and spin the motor. Although disadvantageous in some applications like traditional manipulator arms, it is highly advantageous in quadruped robotics as it allows

impact forces during each step to be absorbed by the motors, increasing energy recovery and reducing stress on the gearbox, softening impact forces and allowing energy to flow back into the battery or be safely dissipated in motor coils, rather than deforming and breaking gear teeth. A low gear ratio helps improve transparency, as it decreases the motor inertia as seen from the load.

In addition, any frictional losses in the gearbox are especially bad for transparency. In the forward direction, as seen by the motor, frictional forces seem exponentially smaller with each additional reducing stage, and thus can be neglected except those in the first stage. However, in the backwards direction, frictional forces get exponentially larger with each stage added. In practice, a gearbox with more than a few stages will not be backdrivable at all - an arbitrarily large force could be applied to the output and it would be completely spent on static friction before even making it back to the input. Real world examples of gearboxes that operate in the backdriven mode, such as mechanical clocks, or other spring driven clockwork mechanisms, overcome this by the combination of maximizing the gear ratio in each stage within the constraints of the manufacturing of fine details (gear teeth) and packaging, and reducing friction as much as possible using cycloidal gear teeth, and carefully designed bearing surfaces to minimize contact area.

Advances in high performance (lightweight and high torque) brushless DC motors developed for drones have significantly mitigated this issue, with many recent quadruped robots using a low gear ratio (Quasi Direct Drive, or QDD) [22] [13] or even pure Direct Drive [23] while still being able to generate enough force to support the robot's weight. This has also had the side effect of increasing backdrivability by reducing the number of reduction stages to one or two.

The third point is maximizing power transfer. A small and agile robot should be able to jump significantly higher than its legs' travel distance, and therefore it must be moving upwards fast enough to reach the desired height on a ballistic trajectory when the foot leaves contact with the ground. Therefore, the amount of energy transferred into the payload mass before the foot leaves the ground should be maximized. It can be seen from the mechanical analog to the maximum power transfer theorem that power transfer is maximized when the impedance of the source and load are equal - i.e. the inertia of the load as seen by the motor through the gearbox is equal to the inertia of the motor's own rotor. Since most motors are optimized to spin at high RPM due to their use in drones, they have low torque and low rotor inertia, and thus require a moderately high gear ratio to lower the load impedance as viewed from the motor enough to be equal to the rotor inertia.

In the example design studied, the ideal gear ratio was found to be 31:1, compared to typical QDD ratios of 3:1 to 9:1. This is problematic, as a gearbox with such a high ratio would either be impractically bulky, add a large amount of inertia to the system, involve more than 1 or 2 stages

and thus preclude backdrivability, or all three. However, a capstan drive-based design can address these problems simultaneously, allowing a single-stage 31:1 reducer to be constructed with much less size and bulk than would be otherwise possible. Using a differential approach as in [12] can increase the reduction ratio even further, but that was not necessary in this case, as the required reduction ratio was possible to achieve in a single, conventional reduction stage.

2.2 Advantages of Capstan Drives Compared to Gear or Belt Transmissions

2.2.1 Limitations of Gears and Timing Belts

Most QDD robots achieve reduction through either a timing belt [13] or planetary gearbox [45][21][3]. These transmissions work well for low gear ratios, but if you try to design one for a larger ratio they quickly become impractical. Both gears (standard or planetary) and timing belts rely on the ratio between the radii of two circles to provide the reduction. Typically, one makes the smaller one, the pinion, as small as practical, and then the size of the other is then determined by the size of the pinion multiplied by the desired gear ratio. However, manufacturing and material strength limitations limit how small the pinion can be.

For gears, smooth running typically requires the pinion have no fewer than about a dozen teeth, and since only a single tooth is in contact at a time, it must be able to bear the full force of whatever impacts may be exerted on the leg without damage, and it can only be so small even if it is made of a strong material like steel.

Similarly, timing belt pinions also have a minimum size of around ten teeth - any smaller and the belt will be bent too tightly and cause excess stress which will damage it. The teeth (and belt) themselves must also be sized adequately to carry the full load. This isn't as severe a constraint as in the case of gears since the load is spread out among many teeth, but the rubber belt teeth are not as strong as steel, and the belt can also stretch slightly, so if the load is too high it will slip. Finally, even if it would be strong enough, the teeth might be too small to be accurately manufactured with a given manufacturing technology - with desktop FDM 3D printing, this limits the size of the teeth to no less than about 1.5 mm wide. Thus for both belts and gears, there is a minimum practical size for the pinion wheel.

While the minimum pinion size is not a problem for low gear ratios, for larger gear ratios the

size of the big wheel to match the pinion quickly becomes impractical. For example, for a 32:1 ratio, a 15 mm diameter pinion would require a ridiculous big wheel 480 mm across - nearly half a meter, and far larger than the entire robot. Alternatively, this could be split up into multiple reduction stages - 3 would work well - but then the friction within the drivetrain would hinder transparency and backdrivabilty.

2.2.2 Advantages of Capstan Drives

One of the main advantages of a capstan drive is the smaller minimum pinion radius, which it can achieve for three reasons. The first is the simpler geometry - the capstan is a simple cylinder, and can thus be made as small as the minimum feature size allows - and can therefore be as small as a single tooth on a gear or timing belt pulley. Radii of < 2 mm are possible even using 3D printing. The second is that there is a much smaller minimum bend radius compared to a belt because unlike a stiff rubber belt, the capstan uses a multifilament braided string. The rubber belt needs to be stiff enough in order to support the teeth which are cantilevered off of it carrying the force, thus limiting the minimum bend radius to significantly more than the tooth size, whereas in the capstan design the force is carried purely by friction between the cable and the capstan. Because the force of the capstan is exponential in winding angle, achieving enough friction between the cable and capstan is easy to achieve even if the material used has a low coefficient of friction, enabling use of low friction high performance polymer fibers like Spectra UHMWPE instead of rubber (reinforced with glass fiber) in the case of belts. And since there is no rubber or other filler material holding the fibers of the cable together, the individual strands can bend individually like in a rope, thus further reducing the minimum bend radius. The 8 strand Spectra fishing line selected here has no trouble achieving the < 2 mm bend radius required. Finally, strength is not impacted by reducing the pinion radius, as it is determined by the inherent strength of the cable only, unlike belts or gears which require teeth large enough to withstand the forces. Thus the small pinion size allows a much larger gear ratio to be achievable in a single reduction stage than with belts or gears, making possible a medium-ratio single-stage transmission design to achieve the simultaneous goals of maximum power transfer, payload capacity, and transparency.

2.2.3 Limits on Capstan Transmission Miniaturizability

The size limits of gear and belt transmissions are well established. What factors limit further miniaturization of capstan drive systems?

The capstan still has to be able to transmit the desired forces and torques to and from the cable, and if it is not strong enough it could deform or break under those loads. And a second, less obvious limitation has to do with the way the cable wraps around the capstan. In most designs, the cable wraps around the capstan between 3 and 6 times before exiting out parallel to the way it entered. This is desirable since it allows the motor to apply force in either direction (since the cable can only sustain tension). However, if it enters the capstan perpendicular to the capstan axis, as might feel natural, it will wrap on top of itself, and thus get tangled and be unable to unwind unless the rotation direction is reversed. This can be solved by wrapping the cable at a slight angle so that it forms a helix with subsequent wraps each laying flat directly on the capstan surface, preferably with at least some gap between them. This wrapping angle depends on the circumference of the capstan and the width of the cable, with a smaller capstan requiring a larger angle. Worse still, since the wraps of cable on the capstan will move up or down the capstan by one cable width per rotation, if a smaller capstan is used with the same radius of big wheel, the capstan will have to rotate more times to move the big wheel through its range of motion. A smaller capstan already has to be longer to account for the increased wrapping angle, and this compounds that effect. This results in a weaker capstan, and increases the required width of the big wheel, increasing its weight and inertia. So there is an eventual limit to capstan size, but if a sufficiently narrow and flexible cable is used, they can be made very small indeed.

In this particular design, a capstan diameter of 4 mm was selected primarily due to process limitations. The motor shaft is 2 mm (standard for this size of motor) and a capstan diameter of 4 mm leaves a wall thickness of only 1 mm, which is about as small a feature as it is possible to reliably form on a standard FDM printer with a 0.4 mm nozzle. Further decreases in diameter would also make it less strong. The cable selected was the smallest size of Spectra fiber readily available, an 8 strand braid with a test strength of 8 lbs and a nominal diameter of 0.150 mm; when pulled flat against the capstan however, the braid tends to flatten, and ends up more like 0.35 mm wide. Considering the wrapping angle, number of wraps, adequate space between wraps, adequate space on each end, and total travel of the actuator (just over 180 degrees), a capstan length of 17 mm was found to be sufficient to avoid tangles.

2.2.4 Cable Material Limitations

The cable is made from Spectra fibers, which are a form of ultra high molecular weight polyethylene (UHMWPE) which has only recently become widely available to consumers in the form of

fishing line. It has some of the highest strength and strength per weight of any known material, and is generally fairly resistant to creep under load, with some versions being especially good [19].

Elasticity under load has the effect of adding an elasticity element in series with the actuator. Some amount of series elasticity is inevitable from an imperfectly stiff frame and leg members, but how much elasticity is desired depends on the overall system design. Additionally, if the transmission is backdrivable, the motor control loop also contributes to effective series elasticity, and by adjusting the proportional term on the motor controller the effective spring constant can be dialed up and down as desired - for example it can be lowered when absorbing an impact to help absorb energy, or increased when more precise or faster motion is needed. [13] [29] However, the energy that can be absorbed in this way is limited by the degree of transparency of the transmission and the power ratings in generating/recharging mode of the motor, controller electronics, and battery system, and so the ability to absorb energy mechanically is valuable. [44]. Too much series elasticity is a problem for making fast and controlled motions, which is why most recent quadrupeds except for anyMAL [17] avoid the use of dedicated series elastic elements. However, a small amount of elasticity has little downsides and can help cushion the worst of peak impact forces from the motor. The selected Spectra fiber is very stiff and doesn't stretch much under its maximum load of 40 N.

Creep - gradual deformation under continuous loading - is another serious concern for cable-driven robots if not addressed. [19] The cables are typically stressed with a high preload since manufacture, and attached with some sort of stiff turnbuckle so that any slight cable stretching would have an immediate effect on cable tension, and in the worst case causing the cable to fall off the capstan under load.

There are several ways of addressing this. The first, the approach taken in [19], which is a highly related design, makes use of a UHMWPE formulation with especially low creep. They found that this was sufficient for their design. The second approach would be to reduce creep by using a larger diameter cable than strictly required. As the cables are so strong and flexible already, this might not negatively impact the design, and also increases the factor of safety against cable failure. The third approach is to use a stiff spring in the cable tensioning system, so that any amount of creep which does occur has a smaller effect on cable preload. This does have the effect of adding mechanical series elasticity, which as discussed above has both positive and negative consequences in and of itself. And finally, one can simply retighten the cables as needed. For a commercial or industrial use robot which must operate for years without maintenance, this might be unacceptable, but for an inexpensive research robot the few seconds it takes to tighten the cable on each actuator with an allen key is not a big issue. This is the approach taken here.

2.2.5 Limits on Capstan Applicability

Unlike belts and gears, capstans are not capable of continuous unlimited rotation, at least not without slipping. Each rotation of the capstan moves the cable wraps up by one cable width, and thus eventually would move it off the end of the capstan. Most kinds of rotational machinery, like vehicles, require continuous rotation, and thus cannot use capstans. However, many robotics applications, including manipulator arms and legs for mobile robots have physical limits to their range of motion, and thus do not require or benefit from continuous rotation, and thus capstans are a good choice considering their other advantages.

2.3 Conclusion

If backdrivability or payload are the driving considerations in transmission design, then they dictate what gear ratio is chosen. However, that ratio may be too low or too high for optimal power transfer, which is what is important for specific agility, a common measure of legged robot performance . Taking this perspective and optimizing the transmission ratio can yield a design which would be impossible to implement using traditional transmission methods, but is possible using a capstan drive as proposed here, enabling better performance from quadruped robots.

Chapter 3

Gravity Compensation

3.1 Introduction

In general, with any sort of robot manipulator arm or leg, when it lifts the load, the robot chassis, or part of the arm itself up against the force of gravity it must do work. In addition, many actuator designs require a constant current draw to produce static torque, even if no work is being performed, so merely holding a weight against gravity may require energy expenditure. If you half squat down, even remaining still there requires constant expenditure of effort, and returning to standing requires additional work to lift up your own weight, and even holding your hand out in front of you requires continual effort. Most robot designs suffer from these very same flaws - there are ways to address them, but they are not themselves without limitations. In the ideal case, with perfect compensation, a robot would expend no energy while standing still, and would only expend precisely the energy required to do the work on the load actually requested. Achieving this in practice is difficult.

3.2 Approaches for Gravity Compensation in Robots

The simplest approach is to not attempt gravity compensation, and instead design an efficient actuator capable of regenerative braking. This provides maximum flexibility, as no restrictions are placed on the robot's kinematics and indeed this approach is taken by most quadruped robots today. However, the round trip efficiency for even an efficient electric motor used in robotics is still pretty miserable, the capabilities are limited by the electrical power ratings, and there remains

a substantial current draw keeping the robot statically supported against gravity. If compensation can be achieved mechanically, then efficiency can be much higher.

3.2.1 Mechanical Gravity Compensation using Masses

There are two broad classes of mechanical gravity compensation - masses and springs [10]. In many ways, mass based compensation is the most straightforward, and often more flexible. The idea is to contrive a way to have a counterweight move in the opposite direction of the load. A classic example would be the counterweight of an elevator, which is attached to the other end of the elevator's cable, and moves down when the elevator moves up and vice versa. Although it cannot compensate for any unknown or variable loads (passengers and cable), it can fully compensate for any known loads such as the self-weight of the elevator. Another example would be in the context of robot manipulator arms, where each link can have a counterweight extending in the opposite direction of the link, partially or fully offsetting the self-weight of the link and other links attached to it. The advantage is that the compensation is independent of the orientation of a joint, which is important in cases where the joint might be at a different angle with respect to vertical depending on the position of upstream joints. The disadvantage is that the mass of counterweight scales linearly with the mass of the downstream links of the arm, and so grows exponentially in the number of links. Additionally, unless the counterweight is allowed to stick out very far to the back, which is often impossible to achieve due to packaging constraints, the counterweight must weigh more than the mass it is counterbalancing, further increasing the compensation required for upstream actuators. And finally, even if gravitational force is compensated, the inertia is still increased, resulting in larger, more powerful actuators being required to achieve the same accelerations. If there happens to be a heavy weight in each link (such as a motor), it can be placed sticking out the back to provide some gravity compensation for free, but it is not an ideal solution for a lightweight and dynamic quadruped.

3.2.2 Spring-Based Gravity Compensation for Agile Robots

The primary advantage of springs is that they are much lighter than a counterweight for a given amount of force. This greatly reduces the exponential compounding of counterweights in long serial chains, and by reducing the inertia of each link, allows them to accelerate faster and operate more safely [25] [41]. The downside of course is that springs do not normally exert a constant force: as most springs are Hookean, the force is linearly related to displacement. This creates

challenges when a spring is used to compensate for a constant force such as gravity - even if it compensates correctly at one place in its range, the force will change throughout the range of motion. Furthermore, if the joint's orientation with respect to gravity changes, then the gravity compensation force required will also change, but the spring will not. Spring-based gravity compensation therefore requires careful design and compromise to achieve the benefits.

3.2.3 Nonlinear Gravity Compensating Systems

In the design proposed here (see Figure 3.1), both of these disadvantages are mitigated. During normal operation, the legs are kept in an approximately vertical orientation, and thus the system's orientation with respect to gravity is kept constant. Furthermore, instead of attempting to compensate each link of the legs individually, we compensate the whole leg system, and thus the changing orientation of each link is not a problem.

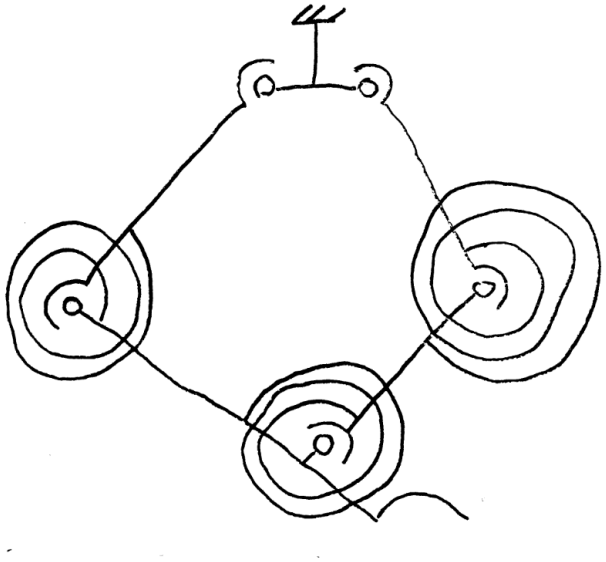

Figure 3.1: Schematic representation of the parallel leg geometry. The two grounded joints at the top are actuated by capstan drives; the remaining joints are passive flexure joints, and hence each have an associated torsion spring, which helps improve energy efficiency and provide gravity compensation

To address the issue of spring linearity, we note that the parallel leg linkage contains a number of rotational joints whose joint angles are highly nonlinear in leg travel. By selecting appropriate stiffness torsion springs to place at each joint, we can produce a leg with an approximately constant force region. Furthermore, if the leg uses flexures in lieu of standard rotational joints, the stiffness

of those joints can be selected to produce the desired spring stiffnesses. The net result is a leg where torsion springs on each joint add or cancel at different points in the leg's travel to produce a near constant force over a wide range of motion, which can be used to compensate for gravity, greatly reducing static loads on the motors, reducing power consumption and enabling use of smaller motors.

One key to making this work is the use of a parallel 5-bar linkage similar to [23] instead of the more common arrangement of either a series linkage or a parallelogram linkage. It turns out that the angles of the ankle and knee joints rotate to broadly cancel each other out and provide a constant force over most of the vertical range of motion - see Figure 3.3.

In the variant explored here, springs were only used on the knee and ankle joints and not on the hip joints. The hip joints, being the only actuated joints in the leg, require ball bearings to stay aligned precisely enough for the capstan drive, whereas more flex and rotation axis drift is acceptable in the other joints. Therefore a spring was not included in the hip joints. As a result, while the spring force is nearly constant along the vertical path directly below the hips, the conditions deteriorate towards the horizontal extremes of travel, and the leg is not statically stable. This should not be a problem, as most quadruped legs don't have any stabilizing springs at all, but if this is desired, springs can also be added to the hips and they further improve the flatness of the energy landscape.

In addition to reducing static power consumption by compensating gravity, the flexure springs form a parallel elastic actuator (PEA) which stores and releases energy during each impact, which should reduce the load on the motor and improve locomotive efficiency [44]. And the additional part count is zero since the flexures have inherent stiffness anyway, and by intentionally choosing the specific stiffness and offset values, they can serve a useful function.

3.2.4 Model of Spring-Compensated 5-bar Linkage

The forward kinematics of a 5-bar linkage are taken from [40] and presented below. After finding all the passive joint angles as a function of the two input joint angles, the spring potential energies can be summed over all of the joints and used to compute the overall potential energy. Gradients can be taken to find the force exerted by the springs throughout the workspace. Finally, by computing the forward kinematics function with slightly displaced input values for the actuator positions, the Jacobian can be found throughout the workspace.

The model, adapted from [40], is shown in Figure 3.2. Parameter values are listed in Appendix

A.

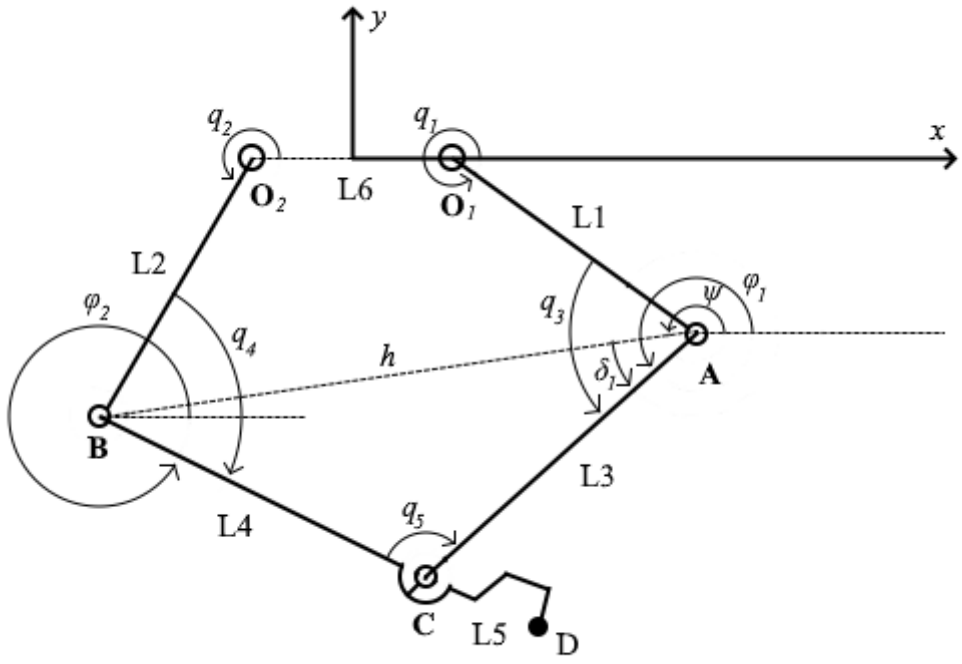

Figure 3.2: Schematic of the 5-bar leg actuator used for the forward kinematics below. Points O_1 and O_2 are fixed to the chassis and contain the only two actuated joints q_1 and q_2. The other three joints are purely passive. Point D is the location of the foot.

The positions (x_A, y_A) and (x_B, y_B) of the knees A and B are

$$x_A = L_1 \cos(q_1) - L_6/2 \tag{3.1}$$

$$y_A = L_1 \sin(q_1) \tag{3.2}$$

$$x_B = L_2 \cos(q_2) - L_6/2 \tag{3.3}$$

$$y_B = L_2 \sin(q_2) \tag{3.4}$$

$$h = \sqrt{(y_B - y_A)^2 + (x_B - x_A)^2}, \tag{3.5}$$

and h is the separation between them. L_1 and L_2 denote the lengths of the front and rear upper leg links, while L_6 is the separation of the two actuated joints, as shown on the diagram.

Next, we make the simplifying assumption that $L_3 = L_4$ - i.e. the two lower leg links are the same length. The sign of the angle δ_1 depends on the configuration of the actuator. In this case, the

knees are bowed out, so we select the positive value,

$$\delta_1 = +\arccos\frac{h}{2L_3}, \tag{3.6}$$

and the other intermediate values shown on the diagram in Figure 3.2 are

$$\psi = \text{atan2}(y_B - y_A, x_B - x_A) \tag{3.7}$$
$$\phi_1 = \delta_1 + \psi \tag{3.8}$$
$$\phi_2 = \pi - \phi_1 + 2\psi. \tag{3.9}$$

The position (x_C, y_C) of the ankle joint C and the position (x_D, y_D) of the foot D are

$$x_C = x_A + L_3\cos\phi_1 \tag{3.10}$$
$$y_C = y_A + L_3\sin\phi_1 \tag{3.11}$$
$$x_D = x_C + L_5\cos\phi_2 \tag{3.12}$$
$$y_D = y_C + L_5\sin\phi_2, \tag{3.13}$$

where L_5 is the length of the offset of the foot from the ankle joint.

Not all input pairs (q_1, q_2) result in a valid configuration. By considering the triangle inequality on $\triangle ABC$, we can discard any input pairs where

$$h > L_3 + L_4. \tag{3.14}$$

The passive joint angles at the knee joints A and B and ankle joint C, which we name q_3, q_4, and q_5, are

$$\angle O_1AC = q_3 = \text{atan2}(y_C - y_A, x_C - x_A) - \text{atan2}(-y_A, -x_A - \frac{L_6}{2}) \tag{3.15}$$
$$\angle O_2BC = q_4 = \text{atan2}(y_C - y_B, x_C - x_B) - \text{atan2}(-y_B, -x_B + \frac{L_6}{2}) \tag{3.16}$$
$$\angle ACB = q_5 = \text{atan2}(y_B - y_C, x_B - x_C) - \text{atan2}(y_A - y_C, x_A - x_C). \tag{3.17}$$

However, joints q_1 and q_2 are the only actuated joints, and q_3, q_4, and q_5 are passive.

The total spring potential energy is

$$U_{spring} = \frac{1}{2}\sum_{i=1}^{5}(q_i - o_i)k_i, \tag{3.18}$$

where o_i is the resting angle and k_i is the spring constant of the ith spring. Gravity can easily be added to this model

$$U_{total} = U_{spring} + mgy_D \tag{3.19}$$

where m is the mass being supported by each leg and g is the gravitational field. Note that y_D is effectively the extension of the leg. The force the leg exerts is

$$F = -\nabla U_{total}(x_D, y_D). \tag{3.20}$$

The Jacobian of the foot position (x_D, y_D) is

$$J = \begin{bmatrix} \frac{dx_D}{dq_1} & \frac{dx_D}{dq_2} \\ \frac{dy_D}{dq_1} & \frac{dy_D}{dq_2} \end{bmatrix}. \tag{3.21}$$

The determinant of the Jacobian $|J|$ can be used to identify when the actuator is near a singularity. In addition to rejecting configurations that violate the triangle inequality. When

$$\text{abs}\left(\frac{1}{|J|}\right) > 0.5 \tag{3.22}$$

we consider it to be too close to a singularity and reject it.

3.2.5 Evaluation of Nonlinear Gravity Compensator Design

The forces can easily be computed using the gradient of the potential energy as a function of the end effector position. Since both the forces under consideration are conservative, their potential energy functions can be computed separately and then added. Gravitational potential energy is very straightforward, simply proportional to the height, but the spring potential energy is more complicated. It can be found by computing the inverse kinematics for each point to get all the joint angles, and then computing the potential energy for each of the joint springs using the joint angles, spring stiffnesses and offsets. The sum of all the potential energies is shown in Figure 3.3

(a) in Cartesian coordinates and in (b) in workspace coordinates (joint angles of the two actuated joints). Note that the flat region of the potential energy function in the middle of the workspace in (a) corresponds to a region of near-zero net force in (d), which shows the sum of the spring and gravitational forces. The formulae for forward and inverse kinematics were from [40].

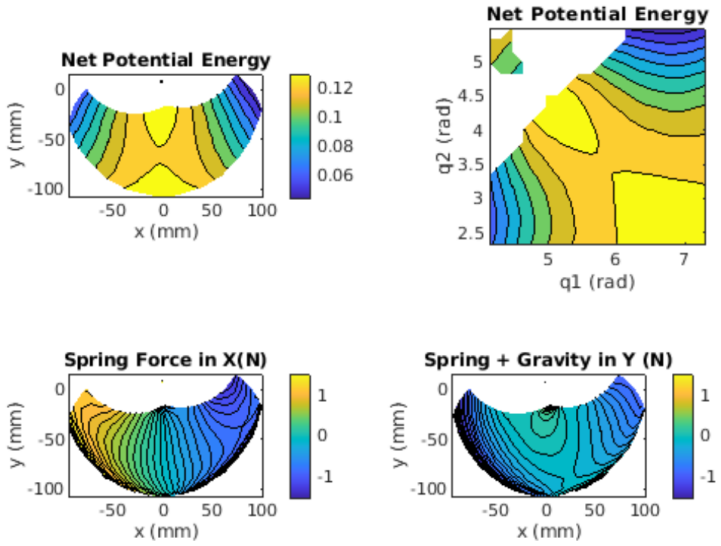

Figure 3.3: Net potential energy is shown in cartesian (a) and workspace (b) coordinates. This is the sum of gravitational and spring potential energy. The sum of spring force and gravitational force is shown in cartesian coordinates in horizontal (c) and vertical (d) components. Note the large region of nearly constant energy in the middle of the workspace corresponding to a region of near zero vertical and horizontal force. This indicates effective gravitational compensation using a linkage creating a nonlinear spring force, at least for the time the actuator spends in that subset of the workspace, which should be most of normal operation judging from typical walking strides of other quadrupeds which make use of a similarly restrictive subset of the workspace during regular operation [17]

3.2.6 Prior Use of 5-bar Linkages in Quadruped Legs

Compared to the biologically-inspired serial linkages, parallel linkages offer the distinct advantage of locating all the heavy motors on the chassis frame, reducing the inertia of the leg. While not technically a parallel linkage, the SOLO-8 leg uses an internal belt within the upper leg to reduce the inertia of a series configuration by locating the motor relatively close to the axis of rotation [13]. In terms of parallel 5-bar linkages, [23] studied two different configurations, the parallelogram configuration, which has seen widespread use, and the symmetric configuration, which according

to them is superior, and has been used among other places in the Minitaur [23] and Stanford Doggo [22].

The design presented here also features a symmetric 5-bar linkage, but with slightly different geometry than the above examples: instead of the two actuated axes being concentric, we located them separated by a small distance (i.e. $L_6 \neq 0$). While this reduces the size of the workspace slightly, this avoids the mechanical complexities associated with having concentric shafts, which was judged to be a worthwhile trade-off.

Parallel elastic actuators (PEA), which are springs operating in tandem with the motor to help support the leg, are relatively uncommon in quadruped robots, and most designs lack them, e.g. [13][23][21]. An example of a PEA in a quadruped leg is a recent paper which proposed adding a spring to the ANYmal quadruped platform [2], with an ellipsoidal cam providing an approximation of the desired non-linearity. The spring provided some gravity compensation, and improved the efficiency, reduced the maximum torque, and increased the runtime [2].

The spring gravity compensation system presented here differs in several important ways:

1. The leg is based on a parallel instead of serial kinematic chain.

2. The desired non-linearity is an inherent result of the linkage geometry, and does not require a separate mechanical component (the cam).

3. The spring forces are generated by flexures instead of dedicated spring elements, reducing part count and simultaneously eliminating an otherwise problematic feature inherent to flexure-based designs.

Although symmetric 5-bar linkages and parallel elastic actuators have been seen in quadruped robotics before, the combination of features presented here appears to be novel.

3.2.7 Conclusion

Spring compensation is superior to mass-based compensation because it is lighter. However, since most springs apply a linear as opposed to constant force, they have a hard time accurately cancelling the constant gravitational force over a large range of motion. Torsion springs mounted on joints of linkages, if correctly designed, can profit from the nonlinear motion of the linkage to produce an approximately constant spring force ideal for compensating the constant gravitational force.

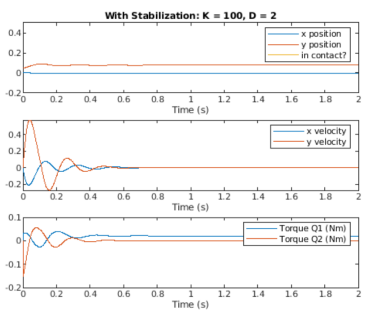

(a) Stabilization with gravity-compensating springs

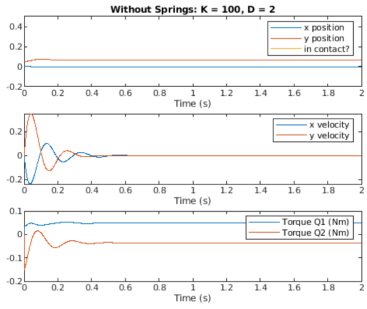

(b) Stabilization without gravity-compensating springs

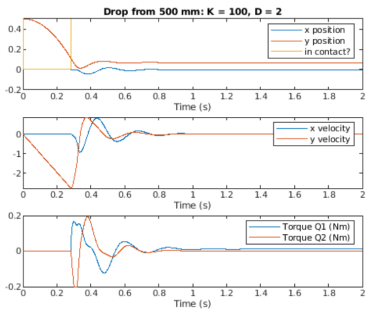

(c) Drop from a height with springs to break the fall

Figure 3.4: Demonstration of the reduction in torque as a result of inclusion of the gravity compensating springs between (a) and (b). Absorbing energy from a fall assisted by the springs is shown in (c). Each sub-figure shows three graphs, showing position, velocity, and actuator torques respectively.

3.3 Control of Nonlinear Gravity Compensated System

Based on a design from a nonlinear control theory course, a dynamic leg model was developed. The model had all the mass localized at the end effector, with link and rotor inertia neglected (see section on impedance matching for a discussion of how to relocate inertia equivalently). However, the full nonlinear leg kinematics were used, and on each frame the joint angles were calculated and used to determine the spring reaction forces; the simulation itself was done in 2D cartesian coordinates. Control is with a simple PID control loop with torque saturation simulated.

Figure 3.4 shows three simulated experimental scenarios. On the left (a) is shown a scenario in which the end effector is commanded to maintain an arbitrary position to simulate the robot's idle pose; there is some oscillation due to the initial position not being the same as the commanded position. In the third graph, showing motor torques, note that both torques stablilze near zero; this is because the commanded position has the force of gravity primarily balanced with springs. When the springs are removed (b) the leg is still able to stabilize at the commanded position, but the final torque values are much higher. This is a result of the springs not compensating for the force of gravity and thus the motor must provide constant torque to do so, drawing unnecessary power and decreasing the life of the motor.

In (c) it is shown a different scenario where the leg is dropped from a height and initially is in freefall, to simulate an impact on the system from a fall or a step. Note that even though the actuator torques do saturate the system is still able to stabilize.

As can be seen in Figure 3.4, springs reduce the static torque loads on the motors, reducing power consumption. Additionally they help absorb (and return) energy during impact, decreasing the peak torque requirements on the motors, and they do not interfere with simple control algorithms.

3.4 Conclusion

Gravity compensation, especially of the counterweight type, is often seen to some extent in fixed manipulator robots as well as non-robot mechanical systems, but is uncommon/unheard of in legged robots due to the weight and inertia penalty. Spring based systems are occasionally studied but are also not commonly used in legged robots, partly due to their linear nature having trouble compensating for a constant force. However, by integrating springs into the joints of a parallel linkage, approximately constant force springs can be simulated without need to resort to specialized components, and can be an effective form of gravity compensation with virtually no downsides.

Chapter 4

Efficient 3D Printing Design Techniques

4.1 Design for 3D Printing

Any material and manufacturing system will have its own limitations and constraints that must be avoided in the design phase to produce a successful design, and 3D printing is no exception. Where 3D printing is special is that it has comparatively few hard constraints on design, and as a result people often either treat it as totally free, or pretend they are designing for another manufacturing paradigm such as injection molding. However, these often lead to unsatisfactory or suboptimal results, and 3D printing as a technology gets unfairly maligned. The following chapter discusses the unique advantages and disadvantages of 3D printing compared to conventional processes like CNC machining and injection molding, and design techniques to best use its advantages and avoid its limitations.

4.1.1 Classification of 3D Printing Technologies

First of all there are multiple types of 3D printing, such as resin (SLA) and powder based methods in either metal or plastic (DMLS, etc), but one of the most popular is Fusion Deposition Modelling (FDM). FDM combines low cost and wide accessibility (vs sintering power based approaches) with good mechanical properties compared to resin printers, at the cost of a rough surface texture and inferior geometrical accuracy. The working principle is that molten plastic (often PLA) is extruded from a mobile nozzle onto a growing part layer by layer, which is the origin of the limitations of the process. A comparison of these processes is shown in Figure 4.1

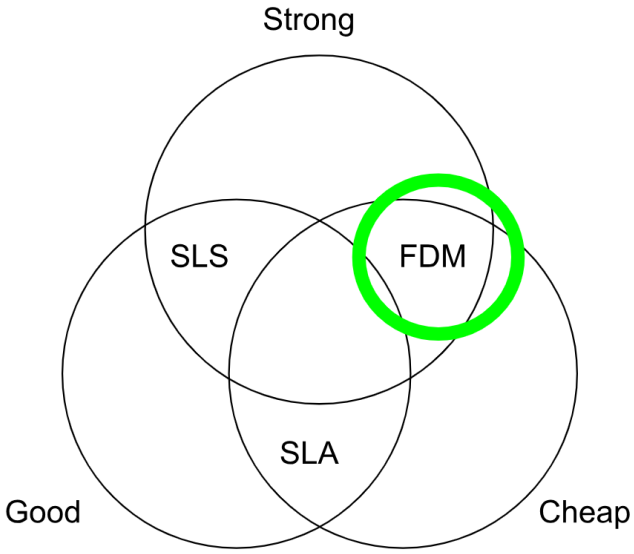

Figure 4.1: General properties of 3 common 3D printing technologies. The popular FDM printing is used here due to its low cost, flexibility, and decent mechanical properties. However, it has worse geometrical accuracy and precision than the other approaches, and a number of limitations on form which must be addressed during the design process.

4.1.2 Strengths of 3D Printing

Let us first discuss the strengths. Because the geometry is formed layer by layer, complex internal geometries and voids are easy to create with few limitations. This stands in contrast to not only conventional manufacturing but also most other types of 3D printing like SLS (selective laser sintering) and SLA. Conventional manufacturing cannot easily create internal voids in monolithic parts: in CNC machining, the part begins as a solid block of material and various tools are used to remove material from the exterior. Internal voids cannot be created as this would require an opening to the outside for the tool to extend through, and indeed any internal geometry more complicated than a straight hole is usually impossible as curved drill bits do not exist. Similarly, creating internal features with precise and well defined geometry is not possible with injection molding as there would be no way to remove the tool forming those features after the part was cast around it. However, blowing air into the mold is widely used to create otherwise impossible internal voids, such as in pop bottles, and works very well for the specific cases it is applicable to, but again is not necessarily suited to complex and arbitrary internal geometries. One would think that other layer-by-layer 3D printing techniques would fare better, and they do, but they still have some limitations. Since SLS involves selectively sintering a bed of powder and SLA uses selective photopolymerization, any voids remain filled with unreacted powder or resin, which needs a way

to leave the part after printing is complete, requiring a hole to be left for this purpose. This is problematic for designs requiring sealed internal voids, or many small internal voids. By contrast, since FDM deposits material only where it is desired in the final part, any voids created have nothing in them but air, requiring no access for postprocessing.

Another strength is that since plastic is extruded along the lines tracing the perimeter of the layer, the each printed line has strength equal to the bulk strength of the plastic used, and if the lines are oriented parallel to the stress, then the part can be as strong as a monolithic piece. However, adhesion between lines either on the same layer or between layers is typically much worse, and the strength is usually about half as good along the vertical direction. It is therefore important to design parts with print orientation in mind to ensure adequate strength; if correctly designed so the stresses run parallel to the print lines, the strength can be excellent.

4.1.3 Design Limitations

Another design limitation is in the form of supports. FDM printing starts on a flat build plate, so all models need to have a flat bottom surface. The ability to extrude plastic into thin air is limited, so each layer must be supported by the layer below. A small amount of overhang is typically acceptable, translating to a maximum overhang angle of 45 to 75 degrees from vertical (significantly more than acceptable in SLA printing), and any overhanging surfaces must conform to this limitation. Additionally, the FDM process is capable of bridging moderately large gaps, provided they are not too long, purely flat (so they are contained within a single layer) and in a straight line. Use of too shallow an overhang angle or too long a bridge results in geometric deviations from the part as designed, variability in manufacture, and in extreme cases total failure of the print.

If the model does not conform to these requirements, then support material can be used. These are 3D printed structures that help support otherwise unsupported sections of the model, and can allow for non-flat undersides of parts, or unsupported regions of models that do not qualify as bridges or sufficiently steep overhangs. Some advanced machines can print these supports in a different material or even a water soluble material, making removal easier, but most printers print support structure in the same material as the main print. This results in additional print time, material waste, degraded surface texture on supported regions of the model, and a great deal of manual labor to remove the support structures. In some cases the supports may not be possible to remove at all, or may require so much force to remove that delicate parts of the model may be

damaged. It is therefore desirable to avoid use of support materials when designing models for 3D printing.

4.1.4 Design for FDM Printing

The first thing to understand about design for 3D printing is that the final product is the result of a collaboration between the 3D CAD package and the slicer. Even for an identical CAD model, changes in the slicer settings can have a huge impact on the appearance, accuracy, strength, and weight of the final part. And finally, the mechanical design of the 3D printer itself can impact how faithfully it can execute the gcode produced by the slicer to place plastic exactly where it is desired and not where it isn't.

Slicing for Efficient Structure

Let's first discuss how slicers process the model into gcode (a sequence of commands for the 3D printer). The model is sliced, dividing the plane into regions that are inside the model and regions that are not, bounded by polygons. For each region, one or more lines are drawn around the perimeter ("walls"), and then if the layer isn't near the top or bottom of the model, the remaining area is filled with a sparse pattern of lines ("infill"). If the layer (or portion thereof) is sufficiently close to the top or bottom of the model, a space-filling curve (commonly back and forth) is used to completely fill the area ("skin"). The result is that the solid model is actually hollow, with the interior filled with low density infill, and the shell thickness determined by the number of walls and number of skin layers. This has a profound impact on the mechanical properties of 3D printed objects, and large implications for how to design for 3D printing.

The stiffness and strength of parts in bending is determined by the second moment of area of the cross section, which is maximized by moving the material as far away from the middle as practical. With conventional fabrication techniques, one is either limited to solid materials, or even if one does make a complex cross section (such as an I-beam or box beam) to increase the stiffness, it either increases cost by increasing machining time, or changes the external geometry, which may be undesired. Furthermore, as the second moment of area is increased by making the e.g. box beam bigger (and walls thinner to hold the cross section constant), the walls will eventually fail in buckling, and require a further hierarchy of stiffeners and other features to prevent buckling, adding additional cost and impracticality. With 3D printing, the internal infill can serve that role, fixing the walls in position and preventing buckling, but not contributing too much additional

weight. Furthermore, the infill can be chosen in the form of a square or triangular lattice, forming an orthogrid or isogrid in the interior, and contributing to the strength of the part as well. The net result is a very high strength to weight part with internal geometry resembling aerospace fabrication techniques like honeycomb composite panels or iso/orthogrid, except without the cost of needing to mill out 90+% of the material, and the flexibility to design structurally efficient parts with a comparatively high degree of geometrical freedom.

An efficient part is therefore one which is physically as large as external constraints permit, provided the resulting walls do not become too thin that the infill required to prevent buckling would be dense enough to significantly increase the weight. As much of the material as possible should be spent on the external walls and skin, as it contributes more to the strength more than material near the inside. The net result is reminiscent of bones - a thin shell with a nearly hollow interior that strengthens the shell against buckling.

Fastening without Hardware

As many features as practical should normally be combined into a single part, but often joining multiple parts together rigidly is still necessary. Conventional methods of fastening such as screws can be used, but can result in an inefficient structure due to the large mismatch in strength and density between steel and 3D printed plastic. Adhesives can also perform well, and match plastic better in terms of strength than steel, but cannot be disassembled, making them less suitable for prototyping, or in general for use in a complex mechanical system which may require servicing or repair. The ideal system, therefore, leverages the low cost of added geometrical complexity of 3D printed parts to build in interlocking features to every part so that forces can be efficiently transferred directly between the parts.

However, even with suitable interlocking features to carry forces, there must still be something to provide the locking force to keep the parts together after assembly. In traditional design, this might be a screw and nut, which can secure not one but a whole stack of parts together. However, there is a mismatch between the volumetric strength of steel and 3D printed largely hollow PLA structures: the plastic surrounding the screw would fail long before the screw itself, leading to a vastly oversized choice of screw (and additional cost and weight). A fastener with a volumetric strength similar to the 3D printed plastic it fastens is therefore desirable; a fastener itself made of 3D printed plastic would be ideal. Unfortunately, the high detail requirements and precision needed for a functional screw make printing a standard screw impossible on all but the largest

scales, and therefore a different technique is called for.

We turn to traditional woodworking and clockmaking for inspiration on geometrically undemanding fasteners in the form of wedges and taper pins. Like a screw, they apply a high mechanical advantage to achieve elastic deformation of the joined pieces, allowing them to remain rigidly attached during either positive or negative loading due to the applied static preload. However, unlike a screw, they do not require small and precise features, and their function is determined by only their overall geometry, making them suited to 3D printing. Their size can also be scaled up and down as appropriate to suit the application.

The design chosen consists of thick plates meeting at the corners with mortise and tenon joints. Compared to a single piece monolithic design, the use of plates allows for better part orientation, since 3D prints are stronger within each layer. Furthermore, it allows a very straightforward way of achieving a stiff and lightweight structure through the use of exposed infill: the top and bottom layers are omitted, as they are not necessary to transmit in-plane forces, and the infill can be set at a desired level of 15%. The mortise and tenon is designed with a 2 degree taper to allow the parts to use a press fit to eliminate any slack or compliance in the joint, while also making assembly easier by not needing to push the joint closed the entire length of the joint, only the last milimeter or so. The taper pins, which can again be 3D printed so that the layers run along their long axis for optimal strength, are inserted into holes in the mortise and tenon joint to lock it all together. This corner joint was found to be insufficiently stiff to bending along the axis of the corner, so a third perpendicular plate was added to brace the joint. The end result can be seen in the Figure 4.2)

4.1.5 Use of Flexures in 3D Printing

3D printing is poorly suited to the creation of bearing surfaces and motion systems primarily due to the large scale of imperfections in the geometry of 3D printed parts: on 3D geometries, the layer lines create an inevitable stairstep texture that can be reduced but not eliminated by using smaller layers, and even on 2D geometries within each layer there will be inevitable surface imperfections due to the seam where the printer transitions between each layer, and often other imperfections caused by retractions (due to needing to move to another section of the part), moisture in the filament, or just general random slubs of plastic, particularly on low-end printers. In addition, common rolling elements like spheres are difficult to 3D print due to the lack of a flat base, and sliding contact between 3D printed surfaces has relatively high friction even in the absence of surface imperfections due to the plastic itself (I measured it to be approximately 0.25), and lubricants

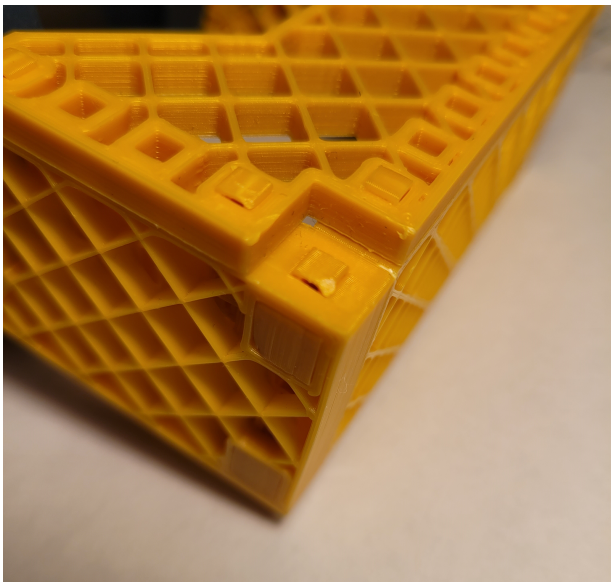

Figure 4.2: Detail of the corner of the frame of the chassis of the 2 DoF Leg Prototype demonstrating an orthogrid structure and a mortise and tenon joint locked with a taper pin

are messy. This is why the vast majority of 3D printed mechanisms either use very loose tolerances (which results in a lot of play) or use commercial ball bearings inserted into 3D printed parts. The former is unsuitable for anything beyond a demonstration model or toy; the latter is highly effective, but inevitably results in bearings vastly overspecified for their loads due to the aforementioned issues with impedance mismatch between the dense metal bearing races and the 3D printed plastic shafts and housings. Where precision and smoothness of motion was required, in the transmission, to maintain accurate separation of the wheel and capstan, this approach was taken, using bearings with an unusually large internal diameter relative to the size of the race to allow enough space inside for enough plastic to support the loads without adding a large amount of unnecessary mass in the form of a thick wall bearing such as a 608. However, where precisely circular motion is not required there is another approach that can be taken: flexures.

A flexure is a geometrical feature of a solid part which is intended to elastically deform in a defined way under load. It is distinct from a living hinge in that it is purely elastic under intended loading conditions, and therefore can be used with any elastic material such as silicon or metal, and does not rely on the material properties of the plastic selected. Through clever geometry, one can simultaneously achieve high stiffness along any undesired degrees of freedom while achieving relatively low stiffness in the desired degree of freedom, and therefore can substitute for conventional linear or rotational joints [33]. A mirrored version of the cross-axis flexure joint [14] was selected due to its simplicity and large range of motion [33].

4.2 Design of a Low-mass 2 DoF Flexure-based Actuator

A 2 DoF Prototype Leg was designed according to the above principles, making use of exposed orthogrid infill, taper pins, and flexure joints (see Figure 4.3). The plates forming the sides and rear of the chassis frame are a small fraction of the mass they would be if they were made of another material, while still being extremely stiff. The other components which appear solid are mostly hollow except for 15% infill, maximizing stiffness by concentrating mass at the exterior. Taper pins are used to hold all the main structural pieces together; M3 screws are used only for attaching the capstan support bracket and as turnbuckles to tension the cable. Likewise, bearings are used only on the main actuated axles of the two wheels; the other joints have cross-axis flexures. The combination of these 3D printing-specific techniques allows a lightweight, stiff, and easy to assemble structure to be made in only a few hours by anyone with a 3D printer.

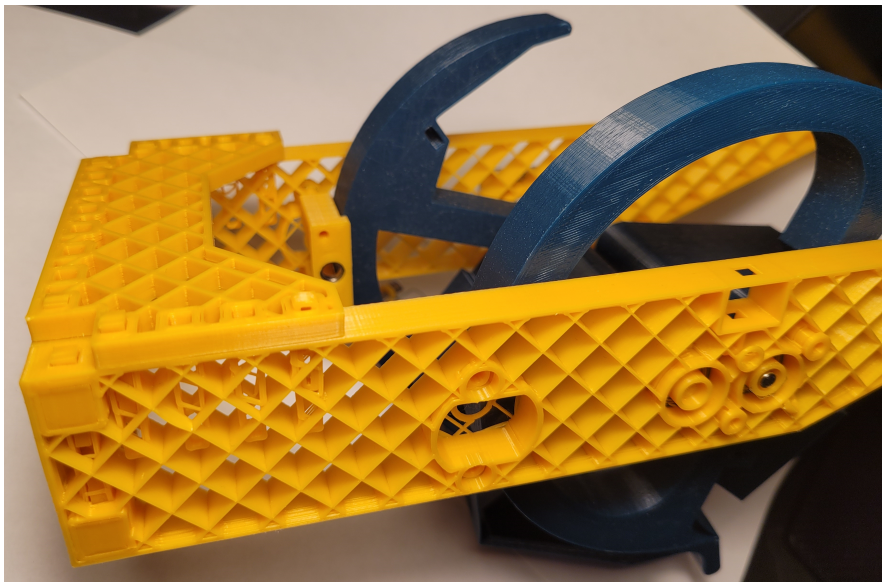

Figure 4.3: Detail of the 2 DoF Prototype showing 3D printed structure techniques.

Chapter 5

Numerical Simulations and Analysis

5.1 1D Simulation

5.1.1 Setup

The first experiment is a simple numerical simulation to confirm the idea of impedance matching. The setup is a very basic one: 1D kinematics, and a constant gear ratio. Plausible values were taken for motor rotor inertia and chassis mass per motor, and the parameters for the standard DC motor model were taken from the motor specifications, with a 6 A maximum current set by the motor driver specified maximum instantaneous current. Integration was done with forward Euler and was cut off when the height reached the nominal leg travel of 10 cm. Based on the final speed at release, the final jump height was calculated. The results of this are shown in the Figure 5.1 below.

In this case, for most of the acceleration phase the motor is current limited, and therefore applying a constant torque resulting in a constant acceleration. When the height reaches 10 cm after only 0.085 seconds, the speed is enough to launch it over 40 cm in the air. The figure on the left shows the simulation of the brushed DC motor with a 2 mm radius capstan, which for the values chosen for motor rotor inertia and load inertia and radius of the big wheel, corresponds to making the rotor inertia equal to the load inertia as seen through the transmission.

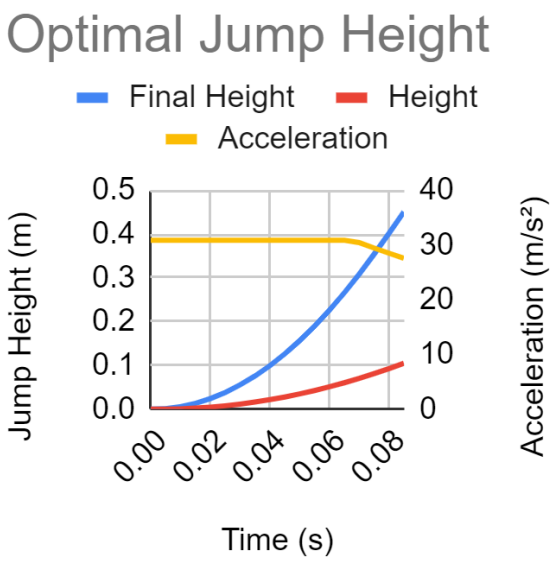

Figure 5.1: Numerical 1D jump simulation using brushed DC motor 1592 (rated 3V, 4A stall, running at 6V, with current capped at 6A, with a capstan radius of 2 mm and a leg travel of 10 cm.

5.1.2 Effect of Gear Ratio

By altering the gear ratio, we can also change the effective inertia of the load as seen from the motor through the transmission; a higher gear ratio makes the load seem smaller and vice versa. However, higher gear ratios also require the motor to spin faster, which in the DC motor model decreases the torque that is available. Moreover, the motor must accelerate more for a given load acceleration, resulting in its own rotor inertia having a greater impact. By contrast, too low of a gear ratio results in the torque applied to the load being low resulting in poor acceleration. The optimal gear ratio is a compromise between high and low gear, which is found when the effective inertia of the motor and load are equal, and indeed this is what was seen in the simulation shown in Figure 5.2 below:

In this figure the maximum jump height is calculated as above, but with varying capstan radii (and thus gear ratio). When the radius is less than 2 mm, the gear ratio is too high and the rotor inertia slows the acceleration too much. Conversely when the radius is greater than 2 mm, the gear ratio is too low and the torque too small to accelerate the load mass quickly enough. When the two inertia are equalized, it accelerates the quickest and reaches the highest speed before leaving the ground.

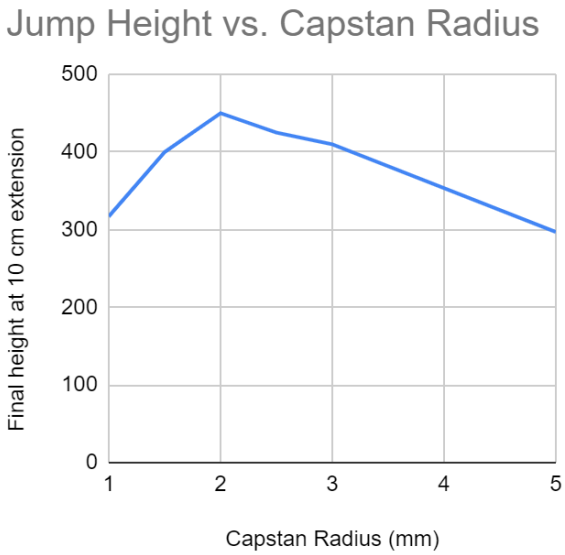

Figure 5.2: For fixed leg travel and motor performance characteristics, choosing the correct capstan radius changes the maximum achievable jump height. The specific performance (jump height) is optimized when the load impedance equals the rotor inertia, which occurs when the capstan radius is 2 mm.

5.1.3 Mathematical Theory

The relevant theory is the mechanical analogue of the maximum power transfer theorem, which states that power transfer is maximized when the impedance of the load is equal to the impedance of the source. In this case, impedance is the sum of inertia (analogous to inductance), damping (resistance) and spring forces (capacitance), and when we neglect damping and spring forces, we get the best power transfer when impedance is equal. The transmission can then be handled the same as an ideal transformer, changing the impedance seen through it by a factor of n^2. [7]

5.1.4 Derivation of Optimal Transmission Ratio

We would like to mathematically derive the optimal capstan radius for use in a quadruped robot leg. We first present a proxy dynamics model for the system, then analyze it. With some further simplifications, it is possible to analytically find the optimal value for the radius, which is precisely the radius which matches the motor and load impedances. The numerical studies demonstrate that even in a more realistic scenario with a more complete motor model, the radius found is still approximately correct.

Problem Definition

We begin by defining a simple linear motor model with capped torque,

$$\tau = min(\tau_{stall}\frac{\omega_{free} - \omega}{\omega_{free}}, \tau_{max}) \tag{5.1}$$

$$\tau_{max} = \frac{j_{max}\tau_{stall}}{j_{stall}} \tag{5.2}$$

which defines the motor torque τ as a function of rotor angular velocity ω and parameters stall current j_{stall}, stall torque τ_{stall} and unloaded rotor angular velocity ω_{free}. This model neglects the no-load current for simplicity, as the motor is operating near stall during the entire trajectory. In addition, the torque output is capped at τ_{max} due to the motor driver having a limited output current j_{max} which is less than the motor stall current, and torque is directly proportional to current.

For the dynamics (5.4 5.5), a simplified 1-D model with constant transmission ratio (represented by the capstan radius r) is used in order to obtain an analytic result. In the real scenario, there would be 2 degrees of freedom, and the ratio would vary somewhat depending on the position in the workspace, but the variation is not that large, justifying this approximation. This is illustrated in Figure 5.3.

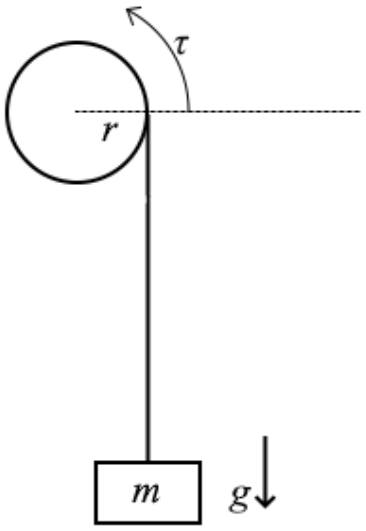

Figure 5.3: Schematic illustration of 1D Capstan Drive

The angular acceleration $\dot{\omega}$ can be found in terms of the torques on the capstan due to the motor

(τ) and weight of the suspended mass $m_{load}g$:

$$\dot{\omega} = \frac{\tau - m_{load}gr}{I_{total}} \tag{5.3}$$

$$I_{total} = I_{rotor} + m_{load}r^2 \tag{5.4}$$

where I_{rotor} is the moment of inertia of the motor rotor and capstan, r is the capstan radius, and m_{load} is the portion of the portion of the mass of the robot allocated to each motor, one eigth the total since the four legs have two motors each. I_{total} is the total rotational inertia of the system, including the load which has been coupled to the capstan by a string. The linear acceleration of the mass m is

$$a(t) = \dot{\omega}r = \frac{\tau r - m_{load}gr^2}{I_{total}}. \tag{5.5}$$

Integrating from rest, the velocity $v(t)$ and height $h(t)$ are simply

$$v(t) = \int_0^t a(t)dt \tag{5.6}$$

$$h(t) = \int_0^t v(t)dt \tag{5.7}$$

If the mass were to continue on a ballistic trajectory beyond time t, then the maximum height reached is

$$h_{max}(t) = \max_{t'>t}(h(t')) = h(t) + \frac{v(t)^2}{2g}, \tag{5.8}$$

as can be seen through energy considerations.

The leg is assumed to lose contact with the ground when the height exceeds the leg travel length l, resulting in the jump height as a function of capstan radius r

$$h_{jump}(r) = \max_{t>0,h(t)<l}(h_{max}(t)). \tag{5.9}$$

Since jump height is the primary design goal, we wish to find the value of r which maximizes it. We are going to show that r^* is such that $m_{load}r^{*2} = I_{rotor}$ — the impedance matched condition — for the case of constant torque and negligible gravity.

Optimal Radius for Constant Torque

In general, the torque available from the motor decreases as the motor speed increases (5.1). However, if the motor drive circuit cannot supply the full stall current of the motor, as is the case here, then the motor current (and hence torque) is effectively capped by the motor driver until the motor speed gets high enough that the motor starts to draw less than that amount of current. One might also choose to limit the current to avoid overheating the motor, driver, or exceeding mechanical loads on the system. However, in this case, these are not a concern due to the very short time span of the jump launch. The motor model simplifies to

$$\tau = \tau_{max} = \tau_{stall}\frac{j_{max}}{j_{stall}}. \tag{5.10}$$

We can now solve the kinematics in terms of the acceleration:

$$\dot{\omega} = \frac{\tau - m_{load}gr}{I_{rotor} + m_{load}r^2} \tag{5.11}$$

$$= \frac{\tau - m_{load}gr}{I_{total}} \tag{5.12}$$

$$a(t) = \frac{\tau r - m_{load}gr^2}{I_{rotor} + m_{load}r^2} \tag{5.13}$$

$$v(t) = \int_0^t a(t)dt = ta \tag{5.14}$$

$$h(t) = \int_0^t v(t)dt = \frac{1}{2}at^2 \tag{5.15}$$

$$h_{max}(t) = \frac{1}{2}at^2 + \frac{a^2t^2}{2g} \tag{5.16}$$

$$\tag{5.17}$$

The leg lifts off the ground at time t_1, when it reaches a height of l, which is the travel distance of the leg:

$$l = h(t_1) = \frac{1}{2}at_1^2 \tag{5.18}$$

$$t_1 = \sqrt{\frac{2l}{a}} \tag{5.19}$$

and since h_{max} is monotonically increasing, the maximum jump height,

$$h_{jump} = h_{max}(t_1) \tag{5.20}$$

$$= h_{max}(\sqrt{\frac{2l}{a}}) \tag{5.21}$$

$$= l + \frac{la}{g} \tag{5.22}$$

occurs at the latest possible point — when the foot leaves the ground.

For a fixed leg length, the jump height is maximized by maximizing the acceleration, which is unsurprising. We can maximize this by taking the derivative of (5.14) with respect to r and finding the root which is at the optimal value:

$$\frac{da}{dr} = \frac{\tau(I_{rotor} + m_{load}r^2) - \tau r(2m_{load}r) - (2m_{load}gr(I_{rotor} + m_{load}r^2) - m_{load}gr^2(2m_{load}r))}{(I_{rotor} + m_{load}r^2)^2} \tag{5.23}$$

$$= \frac{\tau(I_{rotor} - m_{load}r^2) - 2m_{load}grI_{rotor}}{(I_{rotor} + m_{load}r^2)^2} = 0 \tag{5.24}$$

Since the denominator is always positive, we can simply set the numerator equal to zero and obtain the optimal capstan radius r^*:

$$0 = \tau m_{load}r^2 + 2m_{load}gI_{rotor} - \tau I_{rotor} \tag{5.25}$$

$$r^* = \frac{-m_{load}gI_{rotor} + \sqrt{m_{load}^2g^2I_{rotor}^2 + \tau^2 m_{load}I_{rotor}}}{\tau m_{load}}. \tag{5.26}$$

This quadratic produces two real roots, one positive, which we select.

Note that in the case where gravity is negligible compared to the acceleration, this equation reduces to

$$r^* = \sqrt{\frac{I_{rotor}}{m_{load}}} \tag{5.27}$$

which is precisely the condition in which the load and motor inertia are equal:

$$I_{rotor} = m_{load}r^{*2} = m_{load}\frac{I_{rotor}}{m_{load}} \tag{5.28}$$

Indeed, in the case of a high performance agile quadruped, where the expected jump height is significantly more than the leg displacement l, acceleration is typically much higher than g, so this

is a useful approximation. For the example parameters used above, it is only off by about 12% from the optimal value.

Case of Non-Constant Torque

In the case of non-constant torque, we assume the motor is torque limited at first until time t_1, and after that point is able to draw as much current as it desires until it leaves the ground at time t_2. If the motor driver can supply the full stall current of the motor and there is no torque-limited phase, then one can simply set $t_1 = 0$. The torque is given below 5.29:

$$\tau = \begin{cases} \tau_{max} = \tau_{stall}\frac{j_{max}}{j_{stall}}, & \text{if } 0 < t < t_1. \\ \tau_{stall}(1 - \frac{\omega}{\omega_{free}}), & \text{if } t_1 < t < t_2. \\ 0, & \text{if } t > t_2. \end{cases} \tag{5.29}$$

For $t < t_1$, the kinematics are the same as in the previous case (5.17). However, instead of t_1 being the time the foot leaves the ground, it is the point where the motor torque falls below the motor driver maximum.

$$\tau_{stall}\frac{j_{max}}{j_{stall}} = \tau_{stall}(1 - \frac{\omega(t_1)}{\omega_{free}}) \tag{5.30}$$

$$\omega(t) = \frac{v(t)}{r} \tag{5.31}$$

$$\frac{j_{max}}{j_{stall}} = \frac{\omega_{free} - \frac{v(t_1)}{r}}{\omega_{free}} \tag{5.32}$$

$$\omega_{free} - \frac{t_1 a_0}{r} = \omega_{free}\frac{j_{max}}{j_{stall}} \tag{5.33}$$

$$\omega_{free}(1 - \frac{j_{max}}{j_{stall}}) = \frac{t_1 a_0}{r} \tag{5.34}$$

$$t_1 = \frac{r}{a_0}\omega_{free}(1 - \frac{j_{max}}{j_{stall}}) \tag{5.35}$$

where a_0 is the constant acceleration as given in (5.5):

$$a_0 = \frac{\tau_{max} r - m_{load} g r^2}{I_{total}}. \tag{5.36}$$

Substituting that in yields

$$t_1 = \omega_{free}\left(1 - \frac{j_{max}}{j_{stall}}\right)\frac{I_{total}}{\tau_{max} - m_{load}gr}. \tag{5.37}$$

We can now solve the slowing acceleration for time $t_1 < t < t_2$. To begin with, the speed at $t = t_1$ is $a_0 t_1$, so when $t > t_1$

$$v(t) = a_0 t_1 + \int_{t_1}^{t} a(t)dt \tag{5.38}$$

with $a(t)$ being given by (5.5), except this time torque is a function of velocity. Substituting in the speed-dependent torque formula (5.31) yields

$$a(t) = \frac{\tau_{stall}\left(r - \frac{v(t)}{\omega_{free}}\right) - m_{load}gr^2}{I_{total}} \tag{5.39}$$

which, when simplified, results in

$$v(t) = a_0 t_1 + \frac{\tau_{stall}r - m_{load}gr^2}{I_{total}}(t - t_1) - \frac{\tau_{stall}}{I_{total}\omega_{free}}\int_{t_1}^{t} v(t)dt \tag{5.40}$$

Since the expression for $v(t)$ contains an integral for itself, we can solve this by taking the derivative and rearranging, yielding a differential equation

$$\frac{d}{dt}v(t) = \frac{\tau_{stall}r - m_{load}gr^2}{I_{total}} - \frac{\tau_{stall}}{I_{total}\omega_{free}}v(t) \tag{5.41}$$

$$1 = \frac{\frac{d}{dt}v(t)}{\underbrace{\frac{-\tau_{stall}}{I_{total}\omega_{free}}}_{\alpha}v(t) + \underbrace{\frac{\tau_{stall}r - m_{load}gr^2}{I_{total}}}_{\beta}} \tag{5.42}$$

extracting out the coefficients as α and β for convenience:

$$\alpha = \frac{-\tau_{stall}}{I_{total}\omega_{free}} \tag{5.43}$$

$$\beta = \frac{\tau_{stall}r - m_{load}gr^2}{I_{total}} \tag{5.44}$$

whose solution is

$$v(t) = c_1 e^{\alpha t} - \frac{\beta}{\alpha} \tag{5.45}$$

which can be further simplified to

$$v(t) = \left(r - \frac{m_{load}gr^2}{I_{total}}\right)\omega_{free} + c_1 e^{\alpha t} \tag{5.46}$$

where c_1 is shown by velocity continuity at time $t = t_1$ to be

$$c_1 = \frac{a_0 t_1 - \left(r - \frac{m_{load}gr^2}{I_{total}}\right)\omega_{free}}{e^{\alpha t_1}} \tag{5.47}$$

Height for $t_1 < t < t_2$ can then be found by integration.

$$h(t) = h(t_1) + \int_{t_1}^{t} v(t)dt \tag{5.48}$$

$$= h(t_1) + \int_{t_1}^{t} \left(\left(r - \frac{m_{load}gr^2}{I_{total}}\right)\omega_{free} + c_1 e^{\alpha t}\right) dt \tag{5.49}$$

$$= h(t_1) + \frac{c_1}{\alpha}(e^{\alpha t} - e^{\alpha t_1}) + \left(r - \frac{m_{load}gr^2}{I_{total}}\right)\omega_{free}(t - t_1) \tag{5.50}$$

To find the liftoff time t_2 when the leg leaves the ground, we set $h(t_2) = l$ and rearrange:

$$\underbrace{l - h(t_1) + \frac{c_1}{\alpha}e^{\alpha t_1} + t_1\left(r - \frac{m_{load}gr^2}{I_{total}}\right)\omega_{free}}_{d} = \frac{c_1}{\alpha}e^{\alpha t_2} + t_2\underbrace{\left(r - \frac{m_{load}gr^2}{I_{total}}\right)\omega_{free}}_{b}, \tag{5.51}$$

pulling out the constants

$$d = l - h(t_1) + \frac{c_1}{\alpha}e^{\alpha t_1} + t_1\left(r - \frac{m_{load}gr^2}{I_{total}}\right)\omega_{free}$$

$$b = \left(r - \frac{m_{load}gr^2}{I_{total}}\right)\omega_{free}.$$

(5.51) can then be solved by computer yielding

$$t_2 = \frac{\alpha d - b\mathbf{W}\left(\frac{c_1}{b}e^{\frac{\alpha d}{b}}\right)}{\alpha b} \tag{5.52}$$

where W is the Product Log function.

$v(t)$ can be written in terms of the newly defined constants

$$v(t_2) = b + c_1 e^{\alpha t_2}, \tag{5.53}$$

and as before we can reason that due to the positive acceleration, the maximum jump height will occur at the moment the leg leaves the ground (t_2) and therefore by substituting in (5.8) and (5.9) we can obtain a closed form, if long, expression for the maximum jump height even when the torque is not constant.

$$h_{jump} = h_{max}(t_2) = l = \frac{(b + c_1 e^{\alpha t_2})^2}{2g} \tag{5.54}$$

Thus, we have a closed form expression for the jump height as a function of radius (which affects d, α, b, and c_1. This equation can be used to optimize the radius in situations where the constant torque model is a worse approximation, such as with a more powerful motor driver, a longer leg or launch time, or different motor or load characteristics.

5.2 Prototypes

Several prototypes have been built for various different purposes. The two most significant are the 1 DoF capstan test joint, which demonstrated the viability of the capstan transmission system, and the 2 DoF leg prototype, which demonstrated the mechanical design and printing techniques, and illustrated how a capstan transmission might be integrated into a lightweight and low cost 3D printed quadruped robot.

5.2.1 Control and Drive Electronics

For controlling the prototypes and experimenting with them, a simple motor controller for the Pololu 1592 motor was designed based on the DRV8874 motor driver, AS5600 4096-position magnetic encoder, and an ESP32 microcontroller.

The DRV8874 was chosen due to its unusually high peak current rating of 6 A, which was among the highest of the driver chips available for under $15 on Pololu's website. Since one driver chip would be required for each motor, driver chips were expected to be one of the largest components of the cost of the final design, so it made sense for price to be a major consideration. It also had the ability to sense current, which could be useful for force feedback and control algorithms.

The power supply selected is a 2S LiPo battery. With a nominal voltage of 7.2V, it is comfortably more than the 3V nominal voltage of the motor and more than the rated 6V extended range voltage. Since PWM in motor control effectively acts as a variable voltage source, a 7.2 V nominal power supply should be above 6V at all times, and therefore not pose a limit on what the motor will be capable of. For testing of individual leg prototypes the weight, capacity, and current limits were not a major concern, but even for a full quadruped running the 8 motors in 4 legs simultaneously at maximum current (e.g. while jumping) would be possible with a battery under 100 g.

For closed loop control of the actuator position, the original plan was to 3D print an IR optical encoder. 3D printing resolution limited the resolution of such an encoder to a pitch of around 2 mm, which would allow a maximum count per revolution of about 26 in a reasonable diameter. With the high reduction ratio between the capstan and the leg, if this encoder were mounted on the capstan it might be more than accurate enough to monitor the position of the leg for position control. However, ultimately this approach was abandoned due to difficulties running the ADC built into the microcontroller sufficiently quickly given the motor RPM, and other difficulties getting reliable results with the design. The prototype can be seen in Figure 5.4. Instead AS5600 magnetic encoders were selected, which measure the magnetic field of a diametrically magnetized magnet mounted on the shaft of the wheel itself. The 4096 point resolution was better than would have been practical to achieve with the optical encoder even with the reduction ratio of the capstan drive, and as an added benefit provided absolute positioning, eliminating the need for a homing procedure on startup.

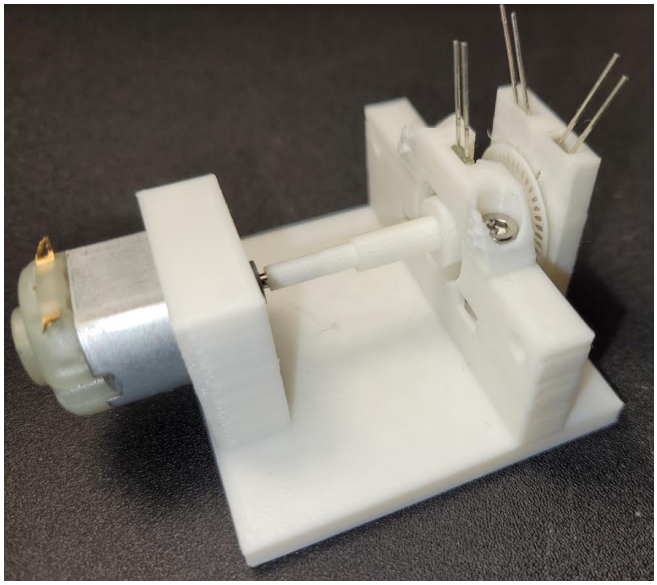

Figure 5.4: Prototype of a 3D printed optical quadrature encoder with integrated capstan (left)

During the planning phase of the project when the scope was more ambitious, the ESP32 controller was selected due to its fast processor and WiFi capabilities, as well as its use in other open source quadruped robot research projects [13]. Ultimately a full quadruped prototype was not produced, and a number of different controllers were used at different points to test different systems, including an Arduino Nano and the ESP32.

5.2.2 Implications of Material Choices

The design is primarily made of two materials: polylactic acid (PLA) for the chassis, capstan, leg, wheels, and fasteners, and ultra-high molecular weight polyethylene (UHMWPE) for the cable. They each affected the design.

The capstan cable must be very strong, as it must carry a substantial preload to avoid slack developing in the system, in addition to the full force of any impacts. UHMWPE is uniquely suited to this task as it has one of the highest strengths of any known material, allowing a cable with sufficient cross-sectional area to be of very small diameter, reducing the minimum bend radius and thus the capstan size. In its commercially available form it is actually a braid of eight individual fibers, resulting in an even smaller bend radius. Steel or titanium cables are not available in such small sizes, and have much larger bend radii as a result, which would make the high ratio capstan drive impossible. Other plastics might work, but would be less strong, have more creep, or have a larger diameter for the same strength, and thus a larger bend radius. Without UHMWPE, this design would not have been possible.

For the 3D printed components, there is more material flexibility. Many plastics have similarly good strength and other material properties, and some, such as acrylonitrile butadiene styrene (ABS) or polyethylene terephthalate glycol (PETG) are also commonly available as 3D printer filament. However, PLA is widely considered to be the easiest material to print with, and as a result parts can be printed on a wider array of printers, and with greater geometric accuracy and fewer defects than with other materials. Other materials, like metal, wood, or carbon fiber, would require a radically different approach to design and would not be able to take advantage of cheap, widely available FDM printers, which were crucial to achieve low cost and easy replicability simultaneously with lightweight structure. So while other plastics are also possible and would likely work similarly well, PLA was chosen because of its good mechanical properties and ease of use.

5.2.3 1 DoF Capstan Test Joint

There were two iterations of the 1 DoF Capstan Test Joint. The first iteration had a fully enclosed case which made the capstan very difficult to wind the thread around, and the capstan also turned out to be too short to consistently avoid tangling. The second iteration (shown in Figure 5.5) had an open design making the capstan easier to access and thread, and it ran smoothly and freely.

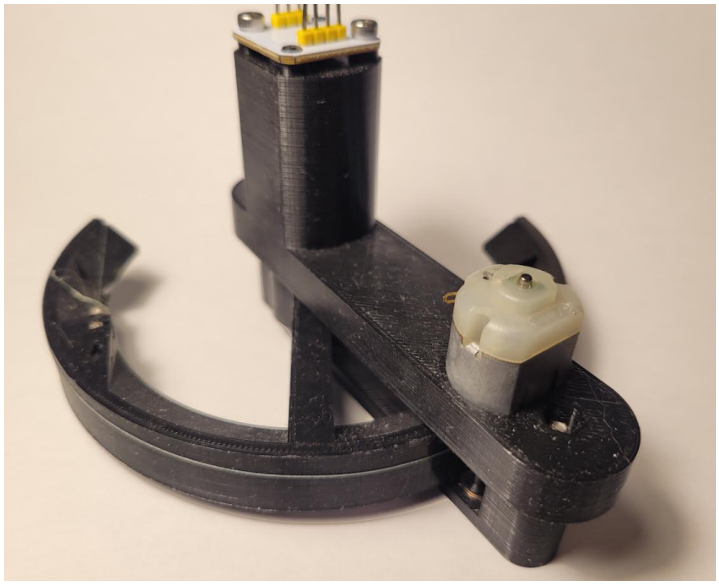

Figure 5.5: 1 DoF 3D printed capstan transmission prototype

5.2.4 2 DoF Leg Prototype

The next step was using the capstan drive as an integrated component in a prototype of a gravity compensating 2 DoF leg based on a 5 bar linkage (Figure 5.6). Such an assembly could be used directly as a single leg on a 8 DoF quadruped dog similar to the original version of the SOLO8 robo [13], or with 1 additional joint to make a 3 DoF leg for use in a full 12 DoF quadruped like the SOLO12 they produced next. This design consists of a 5-bar linkage acting as the leg that was printed as a single piece, with flexures joining 4 distinct rigid bodies and also providing gravity compensation. The unusual shape of the "claw" on the foot was chosen in order to have the clearance to be able to reach up above the hip of the robot to be placed on the toe of the next step in the staircase. The leg is mounted on two parallel axles retained by actual metal ball bearings, which were necessary to ensure they maintained the correct alignment accurately with the capstan, and also spin freely over the necessary range of motion. Lightweight 3D printed plates

held together with mortise and tenon joints retained by taper pins hold all the components in place largely without the need for screws or adhesives. The overall dimensions of the chassis are 240 mm long by 100 mm wide, with a leg stroke of just over 100 mm.

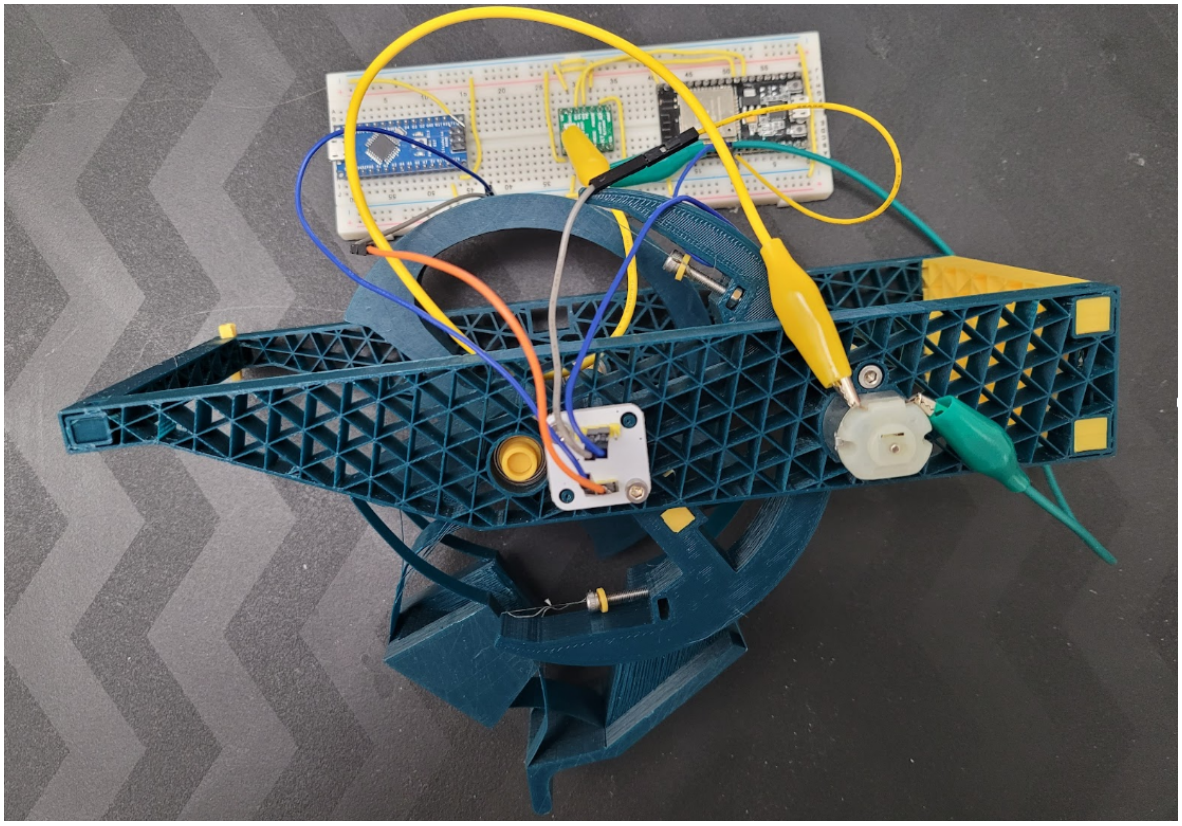

Figure 5.6: The assembled prototype, including the motor, drive, and control electronics

Chapter 6

Conclusion

6.1 Return to Literature

6.1.1 Overview

Quadruped robots are uniquely positioned in the robotics ecosystem, sharing the advantages and disadvantages of both wheeled robots and flying drones, along with their own unique challenges. Chief among these is the fundamental mismatch between high speed low torque electric motors and low speed high force leg motions involved in movement, for which various solutions have been proposed. Generally, these consist of a transmission which puts a fixed ratio between the motor shaft and the leg joint; the choice of this ratio inevitably involves compromising either the transparency or the force output, and results in a robot with heavier motors or worse dynamic performance than might be possible with an optimized design. The unique characteristics of a capstan drive transmission enable it to sidestep the common challenges and achieve a superior design.

6.1.2 Contributions

This thesis focuses on the use of an optimized capstan drive transmission for use in a quadruped leg, and addresses a number of challenges involved in this application:

1. Analysis of transmission ratio, and determining the need for a relatively high transmission ratio.

2. Achieving the high transmission ratio without sacrificing transparency using a capstan drive.

3. Gravity compensation using flexures.

4. Lightweight, fully 3D printed structure.

Taken together, these contributions are key to enabling the design of a much lower cost quadruped than existing designs.

High Ratio Capstan Drive

The primary contribution is on analyzing the problem of small low cost quadruped transmissions from the perspective of optimal power transfer, and realizing that only a capstan drive can achieve the required gear ratio to use such a small and cheap and low torque motor without compromising transparency, adding too much weight, and being possible to package.

Gravity Compensation

The second major contribution was the design of a nonlinear spring based gravity-compensation system which avoids many of the disadvantages found in common spring gravity compensation systems by providing a near-constant force throughout the range of motion, effectively subtracting out the force of gravity on the robot, enabling use of smaller motors, increasing performance, and reducing power consumption. The integrated use of flexures provides the needed spring force while also eliminating the need for additional bearings within the leg joints.

Lightweight 3D Printed Structure

In addition to having a high ratio capstan drive and gravity compensation, the design makes extensive use of 3D printed structure to save on weight and increase reproducibility. Flexures allow fewer parts to be used, as a single part can now encompass multiple independently moving links and not merely a single solid body. And most of the connections between chassis parts are accomplished via 3D printed taper pins, increasing rigidity and lowering weight while also reducing use of non-3D printed components.

Low Cost

Reducing size and cost were guiding motivations for the project from the beginning, and as a result the proposed design is less capable than existing designs which are larger, more powerful, and also multiple orders of magnitude more expensive. Instead of expensive BLDC motors, cheap ($1.50) brushed DC motors which cost 10% of the price are now possible to use. Additionally, the required driver electronics for brushed DC motors is also about 10x cheaper than that required for BLDC motors. Custom machined or fabricated mechanical parts beyond what can be made on an ordinary FDM printer, along with most pieces of hardware like bearings, have been eliminated. The control electronics can also be quite cheap: the popular ESP32 microcontroller can be had for under $10. Together, these should greatly reduce the cost of parts and time required to make a quadrupedal robot from thousands of dollars to hundreds.

6.1.3 Deviations

The design arrived at is quite different than most designs in the literature. These differences are a consequence of the pursuit of the goal of low cost and reproducibility, which rule out many common actuator designs due to motors used and machining required. The biggest differences are in the transmission design, the exclusive use of 3D printed structure, and hence decreased cost and weight, with corresponding tradeoffs in terms of performance.

Choice of Transmission

The choice of capstan drive for quadruped leg actuators is unusual, only seen in [capler], with most designs using either a planetary gearbox or a timing belt-based design, or use a direct drive setup with no transmission at all. This choice limits the maximum gear ratio attainable to below the optimal value, resulting in lost performance, while also weighing more than an equivalent capstan drive. Additionally, these conventional designs require more non-3D printed components due to higher demands on the material.

Use of non-3D Printed Mechanical Components

Other designs take a variety of approaches to structural design. While some, like SOLO [13] do make use of some 3D printed structural components, like the legs, they still make extensive use of non-3D printed components like screws and bearings, and require machine shop access to modify

the 3D printed parts for use as well as modify the motors. Other designs make even less use of 3D printing, instead opting for metal or carbon fiber structures [22]. The proposed design limits the amount of post-processing of 3D printed structures by designing parts which are more tolerant of typical 3D printing defects and process artifacts, and reduces the usage of bearings and screws by using 3D printed functional alternatives - flexures and taper pins. In addition, the capstan drive is more easily printed than a gear or belt based design would be. The resulting design can therefore be produced even without access to a machine shop or metalworking facilities, increasing accessibility and decreasing cost.

Size and Cost

Although prices are not always publicly available, it is widely known that commercial quadrupeds are expensive. Boston Dynamics' Spot Mini is thought to cost around $75K, and even an unassembled kit of the SOLO-12 robot from the Open Dynamic Robotics Initiative costs around $10K. Unitree robots based on the MIT Mini Cheetah are less expensive but still thousands of dollars depending on the model. The fact that this design has the potential to be up to an order of magnitude cheaper than any existing model is a distinguishing feature.

6.1.4 Limitations

The design goals of the project resulted in a number of choices being made differently than in other designs, and some characteristics were sacrificed in order to achieve the design goals, resulting in limitations in the final product. The known and expected limitations of the design include

1. Low performance despite the novel transmission design due to the cheap choice of motor.
2. Expected low durability due to running the motor at higher than rated voltage.

In addition, the project scope and timeline limited the execution of the project, and as a result the implementation of the design did not reach the stage of integrating multiple legs and controlling them like a dog and instead focussed on the design of the transmission and a single leg. Accordingly, there is

1. No complete quadruped prototype, only a prototype of a single leg, similar to [19]
2. The leg itself is incomplete and not tested due to the lack of a testing apparatus, which ended up being beyond the scope of the project.

6.2 Directions for Future Research

Significant work remains in exploring the concept and applications of capstan drives in low cost quadruped vehicles.

6.2.1 Completing and Testing the Prototype

First the leg needs to be integrated. Part of this work has already been completed, including some preliminary test runs of the leg under PID control. These early results were promising, but inconclusive due to the capstan slipping on the motor shaft and the fact that only one of the two leg joints was being controlled. The next steps therefore would be to set up the control electronics for both of the leg joints and test control of the leg as a whole, including with inverse the inverse kinematics developed as part of the gravity compensation section. In addition, a PCB would need to be designed to migrate away from the current unreliable breadboard setup.

With the leg under inverse kinematics control, it would then need to be evaluated for accuracy and repeatability for moving the foot to commanded positions. The next test would be to evaluate the force output and see how high forces it can accurately reproduce, similar to [13]. This would require the addition of a load cell to the test stand. Finally, to test the jump hight, the primary performance measure for a leg in isolation like [19], a test stand which held the leg upright with 1 degree of freedom would need to be made. The leg, weighed down with a mass to simulate its share of the overall payload, would then jump with maximum force over the full range of travel of the leg, thus producing the highest possible jump, which would be the main way of evaluating and comparing the leg to other designs in the literature.

6.2.2 Building a Complete Low-Cost Quadruped

Once the leg was integrated and validated, a chassis integrating four of them, along with a battery and control electronics could be designed. A rounded back, with the battery and payload placed low in the belly, would result in self-righting behaviour despite the limbs' inability to make a complete rotation due to the use of flexures. A grasper arm mounted in the belly would allow the maximum possible payload by keeping the load spread evenly between the four legs.

6.2.3 Adapting Quadruped Control Algorithms

While open loop control might be sufficient for a simple vertical jump [22], more advanced behaviours demand a more involved control scheme, which typically falls into three categories [15]: kinetostatic [5], dynamic, and model-free. Dynamic approaches, including model predictive control (MPC), are the most popular [6] [46], but model-free (learning based) approaches are also increasingly used, especially reinforcement learning (RL) [15][8][43]. Learning on real robots has previously been expensive due to the cost of failures, so most RL is done in simulation [4], possibly with use of trained policies on real robots [18][28] — aided by the use of inexpensive hardware [32][13].

A logical progression would be to evaluate basic leg performance using open loop, position, or torque controlled PID, and then building on top of those control loops to implement some form of kinetostatic control for basic walking. Beyond that, MPC is a popular, general, and robust approach.

6.2.4 Exploring Applications of Low-Cost Quadrupeds

Although intended primarily as a demonstration and research platform, a low cost quadruped could also have a variety of practical uses. Provided it achieved a similar level of mobility in indoor, urban, and off-road environments to other quadrupeds it could be used for similar purposes to its larger brethren provided the payload was sufficiently lightweight. Examples of lightweight payloads involve cameras, thermal cameras, gas sensors, etc. which are all common payloads of industrial robot quadrupeds in practice. In addition, it could be used for extremely lightweight pickup and retrieval tasks, such as litter removal or delivery of very small packages, especially in situations where larger quadrupeds might be too large to operate.

6.3 Conclusion and Larger Implications

The goal of the project was to achieve a 100-fold reduction in cost of capable quadruped robots. While a complete robot was not built, significant progress was made on several of the most pressing problems facing the designers of low cost quadruped robots, in particular in terms of the transmission design and gravity compensation, enabling the use of much cheaper motors and elimination of machining costs - two major contributors to the cost of existing quadruped robots. These insights

will enable future work to achieve the goal of low-cost quadrupeds and all the opportunities that will be opened by them.

Appendix A

Appendix

Proposed Leg Geometry

The parameters for the leg geometry are given in the table below:

L_1	50 mm
L_2	50 mm
L_3	60 mm
L_4	60 mm
L_5	10 mm
L_6	15 mm

Leg segment lengths

	$[rad]$		$[Nm/rad]$
o_1	$1.5\pi + 1$	k_1	0
o_2	$1.5\pi - 0.8$	k_2	0
o_3	1.5	k_3	0.05
o_4	4.6	k_4	0.05
o_5	0.5	k_5	0.05

DC Motor Analysis

Commercially available brushed DC motor performance characteristics were collected and compiled, with the results given in Figure A.1 below. Efficiency is given at peak power output (not peak efficiency). Weight / stall torque is the reciprocal of specific torque, and lower values correspond to a motor that can more easily support itself; this is the most important parameter for motor selection.

DC Motor	Mass (g)	Weight (mN)	Cost (CAD)	Specific Power (\	Power to weight	Weight / Stall tor	Efficiency (%)
RM2	20	196.2	2.85	4.4	0.5	145	21
RM1A	10	98.1	3.09	8.9	0.9	123	36
Pololu 1117	18	176.58	2.21	73.6	7.5	40	51
Pololu 1592	16	156.96	2.21	693.8	70.7	15	44
Adafruit 711	17.7	173.637	2.59	26.4	2.7	89	27
Adafruit 3882	22.4	219.744	2.59	10.3	1.0	88	37
PPN7PA12C1	9.98	97.9038	4.56	106.4	10.8	34	41
M1N10FB11G	17.7	173.637	4.65	54.1	5.5	75	42
PPN13PB11C2	17	166.77	5.06	57.6	5.9	41	42
PWN10VEE24A/	22.3	218.763	5.27	191.2	19.5	18	42
PKN7EB105C7	4.08	40.0248	5.33	154.3	15.7	35	41
PKN12EB105C1	5.44	53.3664	5.65	43.4	4.4	59	40
PNN7RE08JD	2.72	26.6832	5.85	100.4	10.2	53	36
PAN14EE12AA1	39.01	382.6881	6.6	346.7	35.3	11	45
NF123G-301	28	274.68	7.72	82.3	8.4	39	36
NF123G-302	28	274.68	7.44	152.9	15.6	42	35
MABUCHI RS54	160	1569.6	6.17	114.9	11.7	52	33

Figure A.1: Performance, efficiency, and cost metrics computed for a variety of DC motors. Note that the Pololu 1592 has the highest specific power and second-highest specific stall torque despite having the lowest cost.

Bibliography

Bibliography

[1] Biswal, P. and Mohanty, P. K., "Development of quadruped walking robots: A review," *Ain Shams Engineering Journal*, 12(2):2017–2031, 2021.

[2] Bjelonic, F., Lee, J., Arm, P., Sako, D., Tateo, D., Peters, J., and Hutter, M., "Learning-based Design and Control for Quadrupedal Robots with Parallel-Elastic Actuators," 2023.

[3] Bledt, G., Powell, M. J., Katz, B., Di Carlo, J., Wensing, P. M., and Kim, S., "MIT Cheetah 3: Design and Control of a Robust, Dynamic Quadruped Robot," in *IEEE International Conference on Intelligent Robots and Systems*, pages 2245–2252, 2018.

[4] Brunke, L., Greeff, M., Hall, A. W., Yuan, Z., Zhou, S., Panerati, J., and Schoellig, A. P., "Safe Learning in Robotics: From Learning-Based Control to Safe Reinforcement Learning," 2021.

[5] Carius, J., Ranftl, R., Farshidian, F., and Hutter, M., "Constrained stochastic optimal control with learned importance sampling: A path integral approach," *International Journal of Robotics Research*, pages 1–21, 2021.

[6] Carpentier, J. and Wieber, P.-B., "Recent Progress in Legged Robots Locomotion Control," *Current Robotics Reports*, 2(3):231–238, 2021.

[7] Emami, M. R., *Multidisciplinary Engineering Design*, 2018 edition edition, 2018.

[8] Farshidian, F., Hoeller, D., and Hutter, M., "Deep Value Model Predictive Control," pages 990–1004, 2019.

[9] Freschi, C., Ferrari, V., Melfi, F., Ferrari, M., Mosca, F., and Cuschieri, A., "Technical review of the da Vinci surgical telemanipulator," *The International Journal of Medical Robotics and Computer Assisted Surgery*, 9(4):396–406, 2013.

[10] Gosselin, C., "Gravity compensation, static balancing and dynamic balancing of parallel mechanisms," *Smart Devices and Machines for Advanced Manufacturing*, pages 27–48, 2008.

[11] Gosselin, F., Bidard, C., and Brisset, J., "Design of a high fidelity haptic device for telesurgery," in *Proceedings - IEEE International Conference on Robotics and Automation*, volume 2005, pages 205–210, Institute of Electrical and Electronics Engineers Inc., 2005.

[12] Gosselin, F., Ferlay, F., and Janot, A., "Development of a new backdrivable actuator for haptic interfaces and collaborative robots," *Actuators*, 5(2):17, 2016.

[13] Grimminger, F., Meduri, A., Khadiv, M., Viereck, J., Wuthrich, M., Naveau, M., Berenz, V., Heim, S., Widmaier, F., Flayols, T., Fiene, J., Badri-Sprowitz, A., and Righetti, L., "An Open Torque-Controlled Modular Robot Architecture for Legged Locomotion Research," *IEEE Robotics and Automation Letters*, 5(2):3650–3657, 2020.

[14] Haringx, J. A., "The cross-spring pivot as a constructional element," *Applied Scientific Research*, 1:313–332, 1949.

[15] He, J. and Gao, F., "Mechanism, Actuation, Perception, and Control of Highly Dynamic Multilegged Robots: A Review," *Chinese Journal of Mechanical Engineering (English Edition)*, 33(1):1–30, 2020.

[16] Hutter, M., Gehring, C., Bloesch, M., Hoepflinger, M. A., Remy, C. D., and Siegwart, R., "Starleth: A compliant quadrupedal robot for fast, efficient, and versatile locomotion," *Adaptive Mobile Robotics - Proceedings of the 15th International Conference on Climbing and Walking Robots and the Support Technologies for Mobile Machines, CLAWAR 2012*, pages 483–490, 2012.

[17] Hutter, M., Gehring, C., Jud, D., Lauber, A., Bellicoso, C. D., Tsounis, V., Hwangbo, J., Bodie, K., Fankhauser, P., Bloesch, M., Diethelm, R., Bachmann, S., Melzer, A., and Hoepflinger, M., "ANYmal - a highly mobile and dynamic quadrupedal robot," in *2016 IEEE/RSJ International Conference on Intelligent Robots and Systems (IROS)*, volume 2016-Novem, pages 38–44, Institute of Electrical and Electronics Engineers Inc., 2016.

[18] Hwangbo, J., Lee, J., Dosovitskiy, A., Bellicoso, D., Tsounis, V., Koltun, V., and Hutter, M., "Learning agile and dynamic motor skills for legged robots," *Science Robotics*, 4(26), 2019.

[19] Hwangbo, J., Tsounis, V., Kolvenbach, H., and Hutter, M., "Cable-Driven Actuation for Highly Dynamic Robotic Systems," *IEEE International Conference on Intelligent Robots and Systems*, pages 8543–8550, 2018.

[20] Kang, R., Meng, F., Wang, L., Chen, X., Yu, Z., Fan, X., Sato, R., Ming, A., and Huang, Q., "Bio-inspired take-off maneuver and control in vertical jumping for quadruped robot with manipulator," *Micromachines*, 12(10):1–18, 2021.

[21] Katz, B., Carlo, J. D., and Kim, S., "Mini cheetah: A platform for pushing the limits of dynamic quadruped control," in *Proceedings - IEEE International Conference on Robotics and Automation*, volume 2019-May, pages 6295–6301, Institute of Electrical and Electronics Engineers Inc., 2019.

[22] Kau, N., Schultz, A., Ferrante, N., and Slade, P., "Stanford doggo: An open-source, quasi-direct-drive quadruped," in *Proceedings - IEEE International Conference on Robotics and Automation*, volume 2019-May, pages 6309–6315, Institute of Electrical and Electronics Engineers Inc., 2019.

[23] Kenneally, G., De, A., and Koditschek, D. E., "Design Principles for a Family of Direct-Drive Legged Robots," *IEEE Robotics and Automation Letters*, 1(2):900–907, 2016.

[24] Kim, J., Kang, T., Song, D., and Yi, S. J., "PAWDQ: A 3D printed, open source, low cost dynamic quadruped," in *2021 18th International Conference on Ubiquitous Robots, UR 2021*, pages 217–222, Institute of Electrical and Electronics Engineers Inc., 2021.

[25] Kim, Y. J., "Design of low inertia manipulator with high stiffness and strength using tension amplifying mechanisms," in *IEEE International Conference on Intelligent Robots and Systems*, volume 2015-Decem, pages 5850–5856, Institute of Electrical and Electronics Engineers Inc., 2015.

[26] Kljuno, E., Zhu, J. J., Williams, R. L., and Reilly, S. M., "A Biomimetic Elastic Cable Driven Quadruped Robot: The RoboCat," in *ASME 2011 International Mechanical Engineering Congress and Exposition, IMECE 2011*, volume 2, pages 759–769, ASMEDC, 2011.

[27] Konyukhov, A. and Schweizerhof, K., "Frictional Interaction of a Spiral Rope and a Cylinder – 3D-Generalization of the Euler-Eytelwein Formula Considering Pitch," in *Lecture Notes in Applied and Computational Mechanics*, volume 67, pages 413–422, Springer Verlag, 2013.

[28] Lee, J., Hwangbo, J., Wellhausen, L., Koltun, V., and Hutter, M., "Learning quadrupedal locomotion over challenging terrain," *Science Robotics*, 5(47), 2020.

[29] Leziart, P.-A., Flayols, T., Grimminger, F., Mansard, N., and Soueres, P., "Implementation of a Reactive Walking Controller for the New Open-Hardware Quadruped Solo-12," pages 5007–5013, IEEE, 2021.

[30] Lickindorf, D., "Stanley - the capstan based quadruped — Hackaday.io," 2021.

[31] Lickindorf, D., "Stanley at the Van Hack Space - YouTube," 2021.

[32] Lohmann, S., Yosinski, J., Gold, E., Clune, J., Blum, J., and Lipson, H., "Aracna: An open-source quadruped platform for evolutionary robotics," in *Artificial Life 13: Proceedings of the 13th International Conference on the Simulation and Synthesis of Living Systems, ALIFE 2012*, pages 387–392, MIT Press, 2012.

[33] Machekposhti, D. F., Tolou, N., and Herder, J. L., "A review on compliant joints and rigid-body constant velocity universal joints toward the design of compliant homokinetic couplings," *Journal of Mechanical Design, Transactions of the ASME*, 137, 2015.

[34] Raibert, M., Blankespoor, K., Nelson, G., and Playter, R., "BigDog, the Rough-Terrain Quadruped Robot," *IFAC Proceedings Volumes*, 41(2):10822–10825, 2008.

[35] Semini, C., *HyQ - Design and Development of a Hydraulically Actuated Quadruped Robot*, Phd, Italian Institute of Technology, 2010.

[36] Semini, C., Barasuol, V., Goldsmith, J., Frigerio, M., Focchi, M., Gao, Y., and Caldwell, D. G., "Design of the Hydraulically Actuated, Torque-Controlled Quadruped Robot HyQ2Max," *IEEE/ASME Transactions on Mechatronics*, 22(2):635–646, 2017.

[37] Semini, C., Goldsmith, J., Rehman, B. U., and ..., "Design overview of the hydraulic quadruped robots," in *Scandinavian International Conference on Fluid Power*, 2015.

[38] Semini, C., Tsagarakis, N. G., Guglielmino, E., Focchi, M., Cannella, F., and Caldwell, D. G., "Design of HyQ -A hydraulically and electrically actuated quadruped robot," *Proceedings of the Institution of Mechanical Engineers. Part I: Journal of Systems and Control Engineering*, 225(6):831–849, 2011.

[39] Seok, S., Wang, A., Chuah, M. Y., Otten, D., Lang, J., and Kim, S., "Design principles for highly efficient quadrupeds and implementation on the MIT Cheetah robot," in *Proceedings - IEEE International Conference on Robotics and Automation*, pages 3307–3312, 2013.

[40] Shen, H., Liu, Y., Wu, H., Hu, C., and Wang, S., "Forward and Inverse Kinematics for a Novel Double Scara Robot," in *IOP Conference Series: Earth and Environmental Science*, volume 170, page 42088, 2018.

[41] Song, H., Kim, Y. S., Yoon, J., Yun, S. H., Seo, J., and Kim, Y. J., "Development of Low-Inertia High-Stiffness Manipulator LIMS2 for High-Speed Manipulation of Foldable Objects," in *IEEE International Conference on Intelligent Robots and Systems*, pages 4145–4151, IEEE, 2018.

[42] Sun, T., Xiong, X., Dai, Z., and Manoonpong, P., "Small-Sized Reconfigurable Quadruped Robot With Multiple Sensory Feedback for Studying Adaptive and Versatile Behaviors," *Frontiers in Neurorobotics*, 14:14, 2020.

[43] Tsounis, V., Alge, M., Lee, J., Farshidian, F., and Hutter, M., "DeepGait: Planning and Control of Quadrupedal Gaits Using Deep Reinforcement Learning," *IEEE Robotics and Automation Letters*, 5(2):3699–3706, 2020.

[44] Verstraten, T., Beckerle, P., Furnémont, R., Mathijssen, G., Vanderborght, B., and Lefeber, D., "Series and Parallel Elastic Actuation: Impact of natural dynamics on power and energy consumption," *Mechanism and Machine Theory*, 102:232–246, 2016.

[45] Wensing, P. M., Wang, A., Seok, S., Otten, D., Lang, J., and Kim, S., "Proprioceptive actuator design in the MIT cheetah: Impact mitigation and high-bandwidth physical interaction for dynamic legged robots," *IEEE Transactions on Robotics*, 33(3):509–522, 2017.

[46] Winkler, A. W., Bellicoso, C. D., Hutter, M., and Buchli, J., "Gait and Trajectory Optimization for Legged Systems Through Phase-Based End-Effector Parameterization," *IEEE Robotics and Automation Letters*, 3(3):1560–1567, 2018.